

PCCP

Physical Chemistry Chemical Physics

Accepted Manuscript

This article can be cited before page numbers have been issued, to do this please use: J. Tognetti, W. T. Franks, J. R. Lewandowski and S. P. Brown, *Phys. Chem. Chem. Phys.*, 2022, DOI: 10.1039/D2CP01041K.



This is an Accepted Manuscript, which has been through the Royal Society of Chemistry peer review process and has been accepted for publication.

Accepted Manuscripts are published online shortly after acceptance, before technical editing, formatting and proof reading. Using this free service, authors can make their results available to the community, in citable form, before we publish the edited article. We will replace this Accepted Manuscript with the edited and formatted Advance Article as soon as it is available.

You can find more information about Accepted Manuscripts in the [Information for Authors](#).

Please note that technical editing may introduce minor changes to the text and/or graphics, which may alter content. The journal's standard [Terms & Conditions](#) and the [Ethical guidelines](#) still apply. In no event shall the Royal Society of Chemistry be held responsible for any errors or omissions in this Accepted Manuscript or any consequences arising from the use of any information it contains.

Optimisation of ^1H PMLG homonuclear decoupling at 60 kHz MAS to enable ^{15}N - ^1H through-bond heteronuclear correlation solid-state NMR spectroscopy*

View Article Online
DOI: 10.1039/D2CP01041K

Jacqueline Tognetti^{1,2}, W. Trent Franks^{1,2}, Józef R. Lewandowski¹, Steven P. Brown^{2#}

1. Department of Chemistry, University of Warwick, Coventry CV4 7AL, United Kingdom

2. Department of Physics, University of Warwick, Coventry CV4 7AL, United Kingdom

email: S.P.Brown@warwick.ac.uk

* Dedicated to Shimon Vega (1943-2021)

Electronic Supplementary Information (ESI) available: Additional experimental solid-state NMR and simulated data.

Abstract

The Lee-Goldburg condition for homonuclear decoupling in ^1H magic-angle spinning (MAS) solid-state NMR sets the angle θ , corresponding to arctan of the ratio of the rf nutation frequency, ν_1 , to the rf offset, to be the magic angle, θ_m , equal to $\tan^{-1}(\sqrt{2}) = 54.7^\circ$. At 60 kHz MAS, we report enhanced decoupling compared to MAS alone in a ^1H spectrum of ^{15}N -glycine with $PMLG5_{mm}^{\bar{x}\bar{x}}$ at $\theta = 30^\circ$ for a ν_1 of ~ 100 kHz at a ^1H Larmor frequency, ν_0 , of 500 MHz and 1 GHz, corresponding to a high chemical shift scaling factor (λ_{CS}) of 0.82. At 1 GHz, we also demonstrate enhanced decoupling compared to 60 kHz MAS alone for a lower ν_1 of 51 kHz, i.e., a case where the nutation frequency is less than the MAS frequency, with $\theta = 18^\circ$, $\lambda_{CS} = 0.92$. The ratio of the rotor period to the decoupling cycle time, $\Psi = \tau_r / \tau_c$, is in the range 0.53 to 0.61. Windowed $PMLG5_{mm}^{\bar{x}\bar{x}}$ decoupling using the optimised parameters for a ν_1 of ~ 100 kHz also gives good performance in a ^1H spin-echo experiment, enabling implementation in a ^1H -detected ^{15}N - ^1H cross polarisation (CP)-refocused INEPT heteronuclear correlation NMR experiment. Specifically, initial ^{15}N transverse magnetisation as generated by ^1H - ^{15}N CP is transferred back to ^1H using a refocused INEPT pulse sequence employing windowed $PMLG5_{mm}^{\bar{x}\bar{x}}$ ^1H decoupling. Such an approach ensures the observation of through-bond N-H connectivities. For ^{15}N -glycine, while the CP-refocused INEPT experiment has a lower sensitivity ($\sim 50\%$) as compared to a double CP experiment (with a $200 \mu\text{s}$ ^{15}N to ^1H CP contact time), there is selectivity for the directly bonded NH_3^+ moiety, while intensity is observed for the CH_2 ^1H resonances in the double CP experiment. Two-dimensional ^{15}N - ^1H correlation MAS NMR spectra are presented for the dipeptide β -AspAla and the pharmaceutical cimetidine at 60 kHz MAS, both at natural isotopic abundance. For the dipeptide β -AspAla, different build-up dependence on the first spin-echo duration is observed for the NH and NH_3^+ moieties demonstrating that the experiment could be used to distinguish resonances for different NH_x groups.



1. Introduction

Direct ^1H detection is increasingly important for solid-state NMR study of pharmaceuticals¹⁻⁴ and biological molecules.⁵⁻⁸ The availability of ever faster Magic Angle Spinning (MAS) frequencies reduces line broadening due to ^1H homonuclear dipolar couplings.⁹⁻¹⁴ In particular, ^1H detection is advantageous for the identification of specific correlations to nuclei with low gyromagnetic ratio, γ , such as the two natural-abundant isotopes of nitrogen, ^{14}N and ^{15}N . Our focus here is on the spin $I = 1/2$ ^{15}N , though it is to be noted that there is increasing application of ^{14}N - ^1H experiments for the much higher natural abundance (99.6%) spin $I = 1$ nucleus.¹⁵⁻²² The low sensitivity of ^{15}N , associated with its low natural abundance and gyromagnetic ratio, can be overcome by the use of ^{15}N - ^1H correlation experiments with proton acquisition, thanks to the high natural abundance and γ that characterise protons, provided that fast MAS can achieve sufficient ^1H line narrowing.²³⁻²⁶ We note that an ^{15}N -detected MAS-*J*-HMQC ^1H - ^{15}N two-dimensional spectrum has also been recorded at natural abundance and 12.5 kHz MAS using Frequency Switched Lee-Goldburg (FSLG) ^1H homonuclear decoupling.²⁷ ^1H -detected heteronuclear ^{15}N - ^1H correlation experiments can be achieved by inverse polarization, CP, as applied to small molecules^{23,25,26,28-30} and ^{15}N -labelled proteins as a hNH experiment.³¹⁻³³ An alternative to CP-based dipolar-mediated through-space transfer is a *J*-coupling mediated through-bond refocused INEPT solid-state NMR experiment.³⁴⁻³⁷ Specifically, we consider the CP-Refocused INEPT correlation experiment,^{38,39} whereby *J*-coupling mediated ^{15}N - ^1H back-transfer, following CP to give maximum initial ^{15}N magnetisation, ensures only the observation of peaks due to through-bond transfer in a ^{15}N - ^1H spectrum.²⁶ However, fast dephasing due to strong ^1H homonuclear dipolar couplings shortens ^1H coherence lifetimes, reducing sensitivity, making *J*-coupling based experiments challenging. Even 60 kHz MAS is not sufficient to completely average out ^1H homonuclear dipolar couplings.⁴⁰ The application of ^1H homonuclear decoupling⁴¹⁻⁴⁴ under fast MAS during the ^{15}N - ^1H coherence transfer improves sensitivity sufficiently for refocused INEPT transfer.^{26,39}

While a large number of ^1H homonuclear decoupling schemes have been optimised under static conditions for operation at low (5-10 kHz) and moderate (~ 15 kHz) MAS frequencies,⁴¹⁻⁵⁴ there have only been a few papers presenting ^1H homonuclear decoupling at faster MAS frequencies of (35+ kHz)^{55,56} and (60+ kHz).⁵⁷⁻⁶² ^1H homonuclear decoupling is clearly not being applied under quasi-static conditions under such fast MAS and the performance is dependent upon the ratio between the rotor period, τ_r , and the cycle time of the ^1H homonuclear decoupling, τ_c . Lee-Goldburg^{45,46,49,59} and DUMBO^{50,62} based decoupling are characterized by short cycle times which makes them compatible with faster MAS implementations. Nevertheless, a short cycle time means high ^1H nutation frequencies, ν_1 , for the scheme which can be demanding on the instrumentation. In this work, we consider the application of phase-modulated Lee-Goldburg (PMLG)⁴⁹ in a 1D ^1H Combined Rotation and Multiple-Pulse Sequence (CRAMPS)⁶³ experiment at 60 kHz MAS using



relatively low nutation frequencies. The performance of PMLG depends on multiple factors such as the type of PMLG-block, frequency offset, and ^1H nutation frequency;^{41,42,53,54} ^1H homonuclear decoupling sequences are usually evaluated through three principal parameters: the chemical shift scaling factor (λ_{CS}),^{57,58,64} and linewidth improvement reflected in sensitivity and resolution determined through observation of the chemical shift evolution,⁶² and extended coherence lifetimes as observed through echo experiments.⁵⁷ A bimodal Floquet theory analysis shows that ^1H homonuclear decoupling requires a fine optimization at MAS above 40 kHz owing to the considerable number of zero- and first-order degeneracies.⁶⁵ The two types of degeneracy arise when $nv_r + kv_c = 0$, where ν_r is MAS spinning frequency and ν_c is the cycle frequency of the decoupling block, and n and k are integers. When these conditions are met, degeneracies occur within the diagonal block of the Floquet Hamiltonian and the effective Hamiltonian⁶⁶ leading to dipolar line-broadening.

In this paper, we first demonstrate, at 60 kHz MAS, enhanced decoupling compared to MAS alone in a ^1H solid-state NMR spectrum of ^{15}N -glycine for an angle θ , corresponding to arctan of the ratio of the rf nutation frequency, ν_1 , to the rf offset, that is far from the ideal magic angle, θ_m , equal to $\tan^{-1}(\sqrt{2}) = 54.7^\circ$. Moreover, the application of windowed $\text{PMLG5}_{mm}^{\text{xx}}$ decoupling with parameters based on those optimised for the one-pulse spectrum gives enhanced dephasing times in a ^1H spin-echo experiment. In this way, we systematically investigate the ^1H homonuclear decoupling parameters that affect sensitivity in the ^{15}N - ^1H CP-Refocused INEPT experiment under ^1H homonuclear decoupling and fast MAS. It is shown that optimized decoupling enables the recording of two-dimensional through-bond ^{15}N - ^1H MAS NMR correlation spectra for moderately sized organic molecules such as the dipeptide β -AspAla and the pharmaceutical cimetidine.

2. Experimental

^{15}N -labelled glycine, and natural abundance (NA) glycine, β -AspAla and cimetidine were purchased from Sigma Aldrich or Bachem (β -AspAla) and packed as received into 1.3 mm zirconia rotors. ^{15}N -Glycine was packed into a restricted volume in the centre of the rotor using silicone spacers. ^{15}N -labelled glycine was used to optimise ^1H homonuclear decoupling in 1D and 2D correlation experiments and the 2D ^{15}N - ^1H CP-refocused INEPT experiment. Glycine NA and β -AspAla NA were used to test the ^{15}N - ^1H natural abundance CP-refocused INEPT correlation experiment.

The experiments were performed on a Bruker Avance III (500 MHz) or Avance NEO (600 MHz, 1 GHz) spectrometer operating at a ^1H Larmor frequency of $\nu_{\text{OH}} = 500.13$ MHz (11.7 T), 599.45 MHz (14.1 T), 1000.40 MHz (23.5 T) and sample spinning using a Bruker 1.3 mm HXY probe at 60 kHz. The 90° pulse duration of $2.5 \mu\text{s}$ ($\nu_1 = 100$ kHz) for ^1H and $4 \mu\text{s}$ ($\nu_1 = 62.5$ kHz) or $3.5 \mu\text{s}$ ($\nu_1 = 71.4$ kHz, cimetidine) for ^{15}N



was calibrated using a one-pulse experiment and a CP followed by a 90° pulse experiment, respectively. A recycle delay of 3 s or 5 s (cimetidine) was used.

^1H chemical shifts are referenced with respect to tetramethylsilane (TMS) via L-alanine at natural abundance as a secondary reference (1.1 ppm for the CH_3 ^1H resonance) corresponding to adamantane at 1.85 ppm.^{67,68} ^{15}N chemical shifts are referenced relative to liquid CH_3NO_2 at 0 ppm,⁶⁹ using the NH_3^+ peak of glycine (at natural abundance) at -347.4 ppm as a secondary reference. To convert to the chemical shift scale frequently used in protein NMR, where the alternative IUPAC reference (see Appendix 1 of ref. ⁷⁰) is liquid ammonia at -50 °C, it is necessary to add 379.5 to the given values.⁷¹ ^1H and ^{15}N chemical shifts can be experimentally determined to an accuracy of ± 0.2 and ± 0.1 ppm, respectively. The ^{15}N RF transmitter frequency was centred at -304.5 ppm (or -291.5 ppm cimetidine). Where the ^1H resonance offset is referred to, 0 kHz refers to on-resonance with the NH_3^+ peak of glycine at 8.4 ppm, with a positive resonance offset referring to a move of the RF transmitter frequency to higher ppm.

1D CRAMPS. The acquisition window was optimized to acquire 40 complex data points, each corresponding to 0.1 μs , with a ringdown delay of 1.0 μs and a deadtime optimized to be 2.2 μs , corresponding to a total acquisition window, τ_w , of 7.2 μs . The total acquisition time is 15 ms. Both $\text{PMLG5}_{mm}^{\overline{xx}}$ and $\text{PMLG9}_{mm}^{\overline{xx}}$ ^1H homonuclear decoupling schemes were optimized over a ^1H nutation frequency, $\nu_1(^1\text{H})$, range from ~ 10 to ~ 120 kHz.

2D ^{15}N - ^1H CP-Refocused INEPT. Cross polarization (CP) from ^1H to ^{15}N was used for the initial excitation of ^{15}N transverse magnetisation, where the ^1H nutation frequency was ~ 80 kHz (or ~ 95 kHz for cimetidine) using a zero-quantum (ZQ) match condition;⁷²⁻⁷³ and a ^{15}N nutation frequency of ~ 20 kHz (or ~ 25 kHz for cimetidine) with a linear ramp⁷⁴ (70%-100%) on the ^{15}N channel (glycine and β -AspAla) or ^1H (cimetidine). A CP contact time of 2 ms (or 4 ms for cimetidine) was used. The MISSISSIPPI suppression scheme⁷⁵ was applied with a spinlock nutation frequency of ~ 30 kHz for four intervals of 2 ms (or 5 ms for cimetidine) to remove residual ^1H transverse magnetisation. Low-power⁷⁶ heteronuclear ^1H and ^{15}N decoupling was applied during t_1 evolution and ^1H acquisition, respectively, using WALTZ64^{77,78} at a nutation frequency of ~ 10 kHz. The pulse sequence used corresponds to a modified version of that presented by Althaus et al (Fig. 1b).²⁶

Each ^1H -detected FID was acquired for 30 ms with a spectral width of 80 ppm (or 40 ppm for cimetidine). The ^{15}N dimension was acquired with 96 (glycine NA and β -AspAla NA) or 64 (cimetidine) t_1 FIDs with a dwell time of 300 μs (glycine NA) or 142 μs (β -AspAla NA) or 160 μs (cimetidine), corresponding to a ^{15}N spectral width of 66 ppm (glycine NA) or 138 ppm (β -AspAla NA) or 102 ppm (cimetidine) and a maximum t_1 of 15 ms (glycine NA), 6.9 ms (β -AspAla NA), or 5.1 ms (cimetidine). The States-TPPI method was employed to achieve sign discrimination in the indirect dimension.



The pulse sequences, datasets, lists, compound pulse lists, and pulse shapes can be found online at the Warwick online repository, (WRAP *Link*, to be deposited upon acceptance of article).

3. Results and Discussion

3.1 ^{15}N - ^1H CP- refocused INEPT – pulse sequence and product operator analysis

Our implementation of the ^{15}N - ^1H CP- refocused INEPT experiment at 60 kHz MAS is shown in **Fig. 1a**. Note that the pulse sequence in **Fig. 1a** corresponds to a modified version of that used by Althaus et al. at $\nu_r = 40$ kHz.²⁶ The pulse sequence begins with an initial ^1H to ^{15}N CP transfer to provide the largest pool of polarization possible for the low- γ and natural abundance ^{15}N nucleus. The ^{15}N transverse magnetisation is allowed to evolve during t_1 . The desired magnetisation is stored during a z-filter period, in which ^1H magnetisation suppression using the MISSISSIPPI sequence⁷⁵ is implemented to remove the background proton signals. A ^{15}N - ^1H refocused INEPT element is used to transfer the magnetization back to proton for acquisition. INEPT utilizes the ^1H - ^{15}N J -couplings to restrict the signals observed to those with direct one-bond H-N connections. Each spin-echo duration should be an integer number of rotor periods to ensure that the chemical shift anisotropy is completely averaged by MAS. Homonuclear ^1H decoupling, here PMLG,⁴⁹ is applied during the two spin-echoes of the refocused INEPT element. Under fast MAS, at a spinning frequency of 60 kHz in this work, low power heteronuclear decoupling,⁷⁶ specifically WALTZ-64⁷⁸ decoupling, is applied on ^1H and ^{15}N during t_1 and t_2 , respectively. The resulting spectrum is a 2D ^{15}N - ^1H through-bond correlation spectrum, as illustrated in **Fig. 1b** for natural abundance glycine.

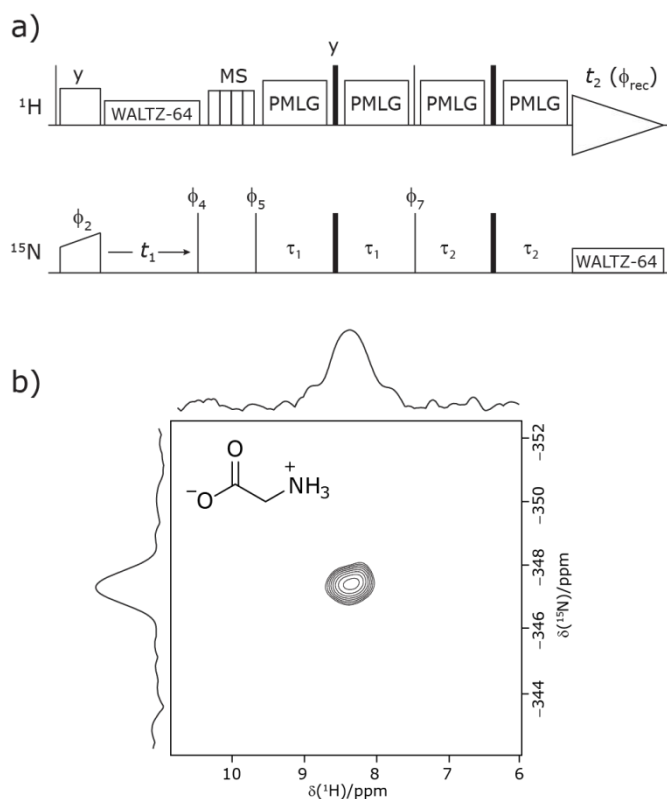


Figure 1. a) Pulse sequence for the ^{15}N - ^1H CP-refocused INEPT experiment utilised in this paper. Narrow lines and filled black rectangles represent $\pi/2$ and π pulses, respectively. Where not stated, the phase of a pulse is x . The following phase cycle is applied: $\phi_2 = \{x^*2, -x^*2\}$, $\phi_4 = \{-y^*4, y^*4\}$, $\phi_5 = \{y^*8, -y^*8\}$, $\phi_7 = \{x, -x\}$ and acquisition $\phi_{\text{rec}} = \{x, -x, -x, x, -x, x, x, -x, -x, x, x, -x, x, -x, -x, x\}$. States-TPPI is implemented on ϕ_4 . b) A ^{15}N - ^1H ($\nu_0 = 500$ MHz) 2D CP (contact time = 2 ms)-refocused INEPT MAS ($\nu_r = 60$ kHz) NMR correlation spectrum with skyline projections of natural abundance glycine and its molecular structure. $\text{PMLG}9_{\text{mm}}^{\text{xx}}$ was applied at a ^1H nutation frequency of 106 kHz ($\tau_{\text{LG}} = 2.92$ μs) during both $\tau_1 = 2.091$ ms (179 τ_c) and $\tau_2 = 0.993$ ms (85 τ_c) at a ^1H transmitter offset of -2.6 kHz, with a zero offset corresponding to being on resonance with the NH_3^+ peak. 192 transients were coadded for each of 96 t_1 FIDs, corresponding to a total experimental time of 16 hours. The base contour is at 40 % of the maximum intensity.

For a ^{15}N - ^1H spin pair, a product-operator analysis (see section S1) shows a product of sine terms dependence on the heteronuclear ^{15}N - ^1H J_{IS} coupling active during the two spin-echo ($\tau - \pi - \tau$) durations, τ_1 and τ_2 :

$$(\text{NH}) \quad \sin(2\pi J_{\text{IS}} \tau_2) \sin(2\pi J_{\text{IS}} \tau_1) \quad (1)$$

i.e., this predicts maximum transfer, for $\sin(\pi/2)$, i.e., $\tau = 1/(4J_{\text{IS}})$, i.e., 2.7 ms, for a one-bond ^{15}N - ^1H scalar coupling (90 Hz) for fast MAS alone. When the proton magnetization is along the transverse plane, for example as $\hat{I}_y \hat{S}_z$ during τ_2 , the ^1H - ^1H dipolar couplings shorten the coherence lifetime compared to when the ^1H magnetization is longitudinal, as during τ_1 .³⁹ As expanded upon below, the different influence of the interactions is evident in the optimum length of the τ_1 and τ_2 periods: the spectrum in **Fig. 1b** was recorded with τ_2 (1.0 ms) shorter than τ_1 (2.1 ms), as discussed further below, note that ^1H homonuclear decoupling scales the J -coupling.⁷⁹⁻⁸¹

Analogously to the case of ^{29}Si - ^1H J couplings in SiH_n moieties,⁸²⁻⁸⁴ there is a different dependence on the first spin-echo duration, τ_1 , for a NH_3 moiety:

$$(\text{NH}_3) \quad \sin(2\pi J_{\text{IS}} \tau_2) [\sin(2\pi J_{\text{IS}} \tau_1) + \sin(6\pi J_{\text{IS}} \tau_1)] \quad (2)$$

As discussed below, a consequence of this is that different signal build-up with respect to τ_1 for a NH and a NH_3 moiety (and also for a NH_2 which has a $\sin(2\pi J_{\text{IS}} \tau_2) \sin(4\pi J_{\text{IS}} \tau_1)$ dependence).

3.2 ^1H PMLG homonuclear decoupling under fast MAS

As noted in the above discussion of **Fig. 1a**, PMLG ^1H homonuclear decoupling is employed during the two spin-echo durations of the refocused INEPT pulse sequence element that transfers magnetisation from ^{15}N to ^1H . Lee-Goldburg decoupling⁴⁵ can be considered to be analogous to MAS where the sample is rotated around an axis inclined at the magic angle, θ_m , equal to $\tan^{-1}(\sqrt{2})$, to the external magnetic field in that the ratio of the nutation frequency, ν_1 , to the resonance offset, $\Delta \nu_{\text{LG}}$, is also set equal to $\tan^{-1}(\sqrt{2})$. This leads to an effective field, $\nu_{\text{eff_LG}}$, that is given by Pythagoras' theorem, as:



$$\nu_{\text{eff_LG}} = \sqrt{\nu_1^2 + \Delta\nu_{\text{LG}}^2}.$$

View Article Online
DOI: 10.1039/D2CP00041K

(3)

For fixed ν_1 , the Lee-Goldburg condition is satisfied as:

$$\tan(\theta_m) = \frac{\nu_1}{\Delta\nu_{\text{LG}}} = \sqrt{2}, \quad (4)$$

i.e., $\Delta\nu_{\text{LG}} = \frac{\nu_1}{\sqrt{2}}$ and $\nu_{\text{eff_LG}} = \sqrt{\frac{3}{2}}\nu_1$. In the PMLG implementation⁴⁹ of the LG condition, rf irradiation is applied on resonance for a duration, τ_{LG} , that is the inverse of $\nu_{\text{eff_LG}}$

$$\tau_{\text{LG}} = \frac{1}{\nu_{\text{eff_LG}}} = \sqrt{\frac{2}{3}} \frac{1}{\nu_1}, \quad (5)$$

but with an equivalent sweep (in discrete jumps) of the rf phase from 0° to ϕ_{last}° over the duration, τ_{LG} , whereby ϕ_{last} depends on $\Delta\nu_{\text{LG}}$ according to:

$$\phi_{\text{last}} = 360^\circ \cdot \Delta\nu_{\text{LG}} \cdot \tau_{\text{LG}} = 360^\circ \cdot \frac{\nu_1}{\sqrt{2}} \cdot \sqrt{\frac{2}{3}} \frac{1}{\nu_1} = \frac{360^\circ}{\sqrt{3}} = 207.8^\circ. \quad (6)$$

An overall rotation, ξ_{LG} , of 360° around the effective field is achieved:

$$\xi_{\text{LG}} = 360^\circ \cdot \nu_{\text{eff_LG}} \cdot \tau_{\text{LG}} = 360^\circ. \quad (7)$$

In the experimental implementation of PMLG under MAS, the duration over which the phase is swept (as discrete steps) from 0° to the ideal ϕ_{last} value of 207.8° , $\tau_{\text{LG_expt}}$, can vary from the ideal value, τ_{LG} . In this way, the equivalent resonance offset, $\Delta\nu_{\text{expt}}$, changes from the ideal value, $\Delta\nu_{\text{LG}}$, to satisfy:

$$\phi_{\text{last}} = \frac{360^\circ}{\sqrt{3}} = 360^\circ \cdot \Delta\nu_{\text{LG_expt}} \cdot \tau_{\text{LG_expt}}, \text{ so that } \Delta\nu_{\text{LG_expt}} = \frac{1}{\sqrt{3}\tau_{\text{LG_expt}}}.$$

Nishiyama et al.⁵⁷ have shown that this deviation from the ideal condition can be expressed in terms of how the angle, θ , deviates from the magic angle, θ_m :

$$\theta = \tan^{-1}\left(\frac{\nu_1}{\Delta\nu_{\text{LG_expt}}}\right) = \tan^{-1}\left(\nu_1 \cdot \tau_{\text{LG_expt}} \cdot \sqrt{3}\right). \quad (8)$$

The actual effective field, $\nu_{\text{eff_LG_expt}}$, that is calculated by Pythagoras' theorem as $\sqrt{\nu_1^2 + \Delta\nu_{\text{LG_expt}}^2}$ is not equal to $1/\tau_{\text{LG_expt}}$ and also deviates from the ideal value, $\nu_{\text{eff_LG}}$. As a consequence, the overall rotation about the actual effective field, $\xi_{\text{LG_expt}}$, also deviates from $\xi_{\text{LG}} = 360^\circ$ according to:



$$\xi_{\text{LG_expt}} = 360^\circ \cdot \nu_{\text{eff_LG_expt}} \cdot \tau_{\text{LG_expt}} = 360^\circ \cdot \sqrt{\nu_1^2 + \frac{1}{3\tau_{\text{LG_expt}}^2}} \cdot \tau_{\text{LG_expt}} \quad (9)$$

View Article Online
DOI: 10.1039/D2CP01041K

Note that Nishiyama et al. refer to this rotation angle as ψ , but this symbol is used in this paper to denote the ratio of the rotor period to the cycle time (see later discussion), according to Leskes et al.⁶⁵

Following the notation of Leskes et al.⁸⁵ a PMLG block is specified as $PMLGn_R^\phi$, where: first, n is the number of finite pulses for each LG cycle, with n equal to 5 or 9 investigated here; second, R is the sense of the initial rotation for the phase steps, m for clockwise and p for counter-clockwise; and third, the initial phase, ϕ , is usually x or $-x$ (denoted \bar{x}). As stated above (see eq. 7) and as shown in **Fig.2a** and **2b**, $\tau_{\text{LG_expt}}$ is the time to sweep the phase over n discrete steps, i.e., as n finite pulses, from 0° to 207.8° . A single PMLG block, $PMLGn_R^\phi$, is of duration $2\tau_{\text{LG}}$ with a 180° jump after n finite pulses in the first τ_{LG} followed by n finite pulses in the second τ_{LG} , whereby the phase steps are in the opposite direction. This corresponds to changing the sign of the equivalent resonance offset, as in the frequency-switched (FS) LG experiment, where rf irradiation is alternated between $+\Delta\nu_{\text{LG}}$ and $-\Delta\nu_{\text{LG}}$.^{46,86,87} As further shown by Leskes et al.⁸⁵ supercycling can be achieved as $PMLGn_{RR}^{\phi\phi}$. Specifically, in this work, we use the $PMLG5_{mm}^{\bar{x}x}$ and $PMLG9_{mm}^{\bar{x}x}$ implementations.



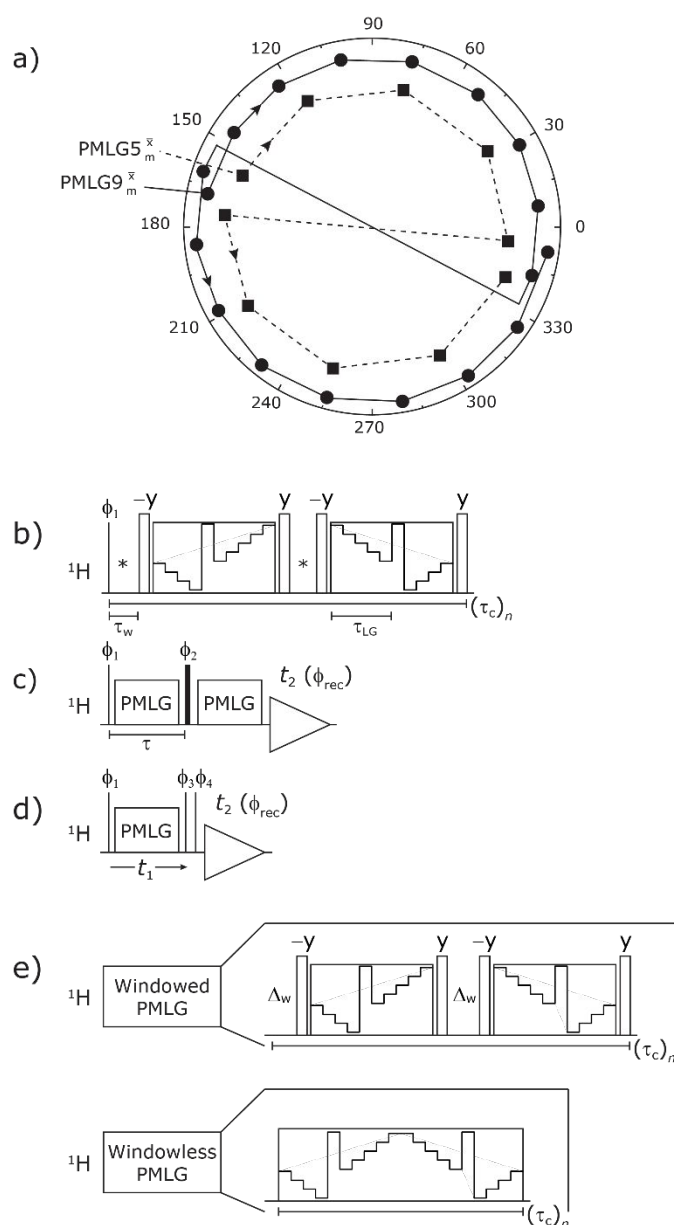


Figure 2. a) Representation of the phase rotation for $PMLG5_m^{\bar{x}}$ (dashed line, squares) and $PMLG9_m^{\bar{x}}$ (solid line, circles). The phase increments are calculated according to $\phi_{\text{last}} = 207.8^\circ$ (see eq. 6), divided by the number of steps. The starting point for both is $-x$. Pulse sequence for b) a ^1H 1D CRAMPS experiment with supercycled $PMLG5_m^{\bar{x}}$, where the asterisk represents an acquisition window, τ_w , c) a ^1H spin-echo and d) a 2D ^1H - ^1H correlation experiment. Thin lines and filled rectangles represent 90° and 180° pulses, respectively, while open rectangles denote tilt pulses. In c) and d), the block named PMLG can accommodate either a e) windowed, where τ_w is an equivalent period of free evolution, or a windowless sequence, whereby there is continuous rf irradiation during $PMLGn_R^\phi$ blocks, i.e., there are no tilt pulses and $\tau_w = 0$. The following phase cycle is applied for b) 1D CRAMPS: $\phi_1 = \{x, -x, -x, x\}$, $\phi_{\text{PMLG}} = \{x, -x, -x, x\}$ and acquisition $\phi_{\text{rec}} = \{x, -x, -x, x\}$; c) ^1H spin-echo: $\phi_1 = \{x, -x\}$, $\phi_2 = \{y^*2, x^*2\}$, $\phi_{\text{PMLG}} = \{x, -x\}$ and acquisition $\phi_{\text{rec}} = \{x, -x, -x, x\}$; d) ^1H - ^1H homonuclear correlation: $\phi_1 = \{x, -x\}$, $\phi_3 = \{-x^*2, x^*2\}$, $\phi_4 = \{x^*4, y^*4\}$, $\phi_{\text{PMLG}} = \{x, -x\}$ and acquisition $\phi_{\text{rec}} = \{x, -x, -x, x, y, -y, -y, y\}$.



In the windowed implementation of PMLG⁸⁸ acquisition windows of duration τ_w are placed between the $PMLGn_R^\phi$ blocks (see **Fig. 2b** and **2e**). In addition, tilt pulses of duration τ_{tilt} can be used.^{53,89-92} The cycle time for a complete $PMLG5_{mm}^{\bar{x}}$ or $PMLG9_{mm}^{\bar{x}}$ supercycle, τ_c , is:

$$\tau_c = 2\tau_w + 4\tau_{\text{LG_expt}} + 4\tau_{\text{tilt}}. \quad (10)$$

3.3 Optimisation of CH₂ and NH₃ signal intensity in a 1D CRAMPS experiment of ¹⁵N-glycine

The optimization of the ¹H nutation frequency and $\tau_{\text{LG_expt}}$ is performed differently for windowless and windowed sequences. In this paper, our focus is on windowed sequences that were optimized with a 1D CRAMPS experiment which gives both the chemical shift scaling factor λ_{CS} and the ¹H linewidths in a few seconds for a particular combination of parameters. Specifically for windowed $PMLG5_{mm}^{\bar{x}}$ and $PMLG9_{mm}^{\bar{x}}$, a two variable optimization was performed over a range of ¹H nutation frequencies between 0 and 110-120 kHz and $\tau_{\text{LG_expt}}$ between 3.5 and 7.5 μs for ¹⁵N labelled glycine – see **Fig. 3a** for $PMLG5_{mm}^{\bar{x}}$ and **Fig. S1** with slices extracted at different peak intensities, hence with different resolution. (Note that the optimisation of the tilt pulses is discussed in section S3 of the Supporting Information.) For windowless sequences, a coarse optimization was performed, starting from optimised parameters from the 1D CRAMPS experiments, using a ¹H spin-echo experiment (**Fig. 2c**) to find good candidate parameters which yield a long ¹H coherence lifetime. As noted below, the ¹H-¹H correlation experiment (**Fig. 2d**) was used to determine the λ_{CS} of the candidate sequences, but can only be used sparingly as the experimental time is relatively long (~20 minutes for 4 co-added transients and 96 t_1 FIDs for each combination of $\tau_{\text{LG_expt}}$ and ν_1).

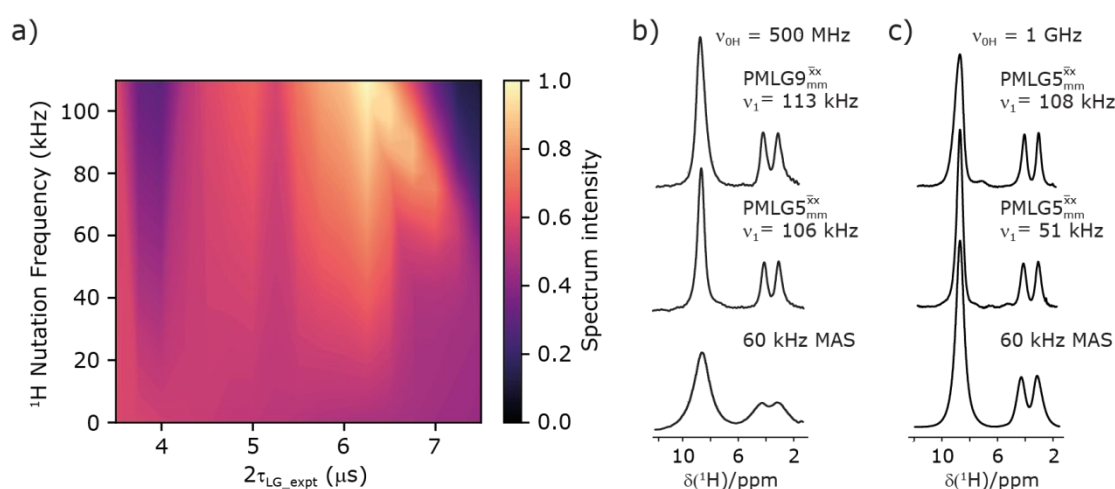


Figure 3. ¹H MAS ($\nu_r = 60$ kHz) NMR of ¹⁵N-labelled glycine. a) $PMLG5_{mm}^{\bar{x}}$ 1D CRAMPS (see **Fig. 2b**, $\tau_{\text{tilt}} = 0.54$ μs , $\Omega = -0.6$ kHz) two-variable optimization ($\nu_0 = 500$ MHz) of both $\tau_{\text{LG_expt}}$ (in steps of 0.25 μs) and the ¹H nutation frequency, ν_1 (0 kHz – 110 kHz) for the NH₃⁺ peak intensity. b) Comparison between ¹H ($\nu_0 = 500$ MHz) 1D CRAMPS MAS NMR



spectra acquired with windowed $PMLG9_{mm}^{xx}$ ($\nu_1 = 113$ kHz, $\tau_{LG_expt} = 2.92$ μ s, $\tau_{tilt} = 0.82$ μ s, $\Omega = -0.6$ kHz), windowed $PMLG5_{mm}^{xx}$ ($\nu_1 = 106$ kHz, $\tau_{LG_expt} = 3.1$ μ s, $\tau_{tilt} = 0.54$ μ s, $\Omega = -0.6$ kHz), and a one-pulse MAS-alone experiment. c) Comparison between 1H ($\nu_0 = 1$ GHz) 1D CRAMPS MAS NMR spectra acquired with windowed $PMLG5_{mm}^{xx}$ ($\nu_1 = 108$ kHz, $\tau_{LG_expt} = 3.10$ μ s, $\tau_{tilt} = 0.18$ μ s, $\Omega = -7.0$ kHz), windowed $PMLG5_{mm}^{xx}$ ($\nu_1 = 52$ kHz, $\tau_{LG_expt} = 3.63$ μ s, $\tau_{tilt} = 0.70$ μ s, $\Omega = -8.6$ kHz), and a one-pulse MAS-alone experiment. 8 (a) or 32 (b and c) co-added transients were added for a recycle delay of 3 s. For all experiments, $\tau_w = 7.20$ μ s.

Figure 3a reports on the NH_3^+ 1H resonance, noting its relevance in this paper for the 1H - ^{15}N refocused INEPT experiment. Figure S2 shows that optimum performance for the NH_3^+ 1H resonance (**Fig. S2b**) is closely matched by that for the CH_2 1H resonances (**Fig. S2a**). 1D CRAMPS 1H NMR spectra of ^{15}N -glycine for our best implementations of supercycled windowed $PMLG5_{mm}^{xx}$ and $PMLG9_{mm}^{xx}$ at $\nu_0 = 500$ MHz are shown in **Fig. 3b**, where enhanced resolution compared to MAS alone is evident. Moreover, both $PMLG5_{mm}^{xx}$ and $PMLG9_{mm}^{xx}$ implemented at $\nu_0 = 500$ MHz (**Fig. 3b**) show better resolution than 60 kHz MAS alone at $\nu_0 = 1$ GHz (**Fig. 3c**). At $\nu_0 = 1$ GHz, optimised 1D CRAMPS 1H NMR spectra of ^{15}N -glycine for windowed $PMLG5_{mm}^{xx}$ at a 1H nutation frequency of 108 and 51 kHz are presented in Fig. 3c that show enhanced resolution compared to MAS alone. Note that the latter case corresponds to the nutation frequency being less than the MAS frequency.

Table 1 compares the experimentally optimised τ_{LG_expt} values to the ideal τ_{LG} values: at $\nu_0 = 500$ MHz, the experimental values are less than half the ideal values, i.e., $\tau_{LG_expt} = 3.10$ μ s and 2.92 μ s compared to 7.70 μ s and 7.23 μ s, respectively. As **Table 1** further shows, with the corresponding changes in $\Delta\nu_{LG_expt}$ and ν_{eff_expt} , the angle θ is 29.7° , respectively. While a very high nutation frequency of over 200 kHz has been used in the first experimental implementations of PMLG at 65 kHz MAS frequency^{59,65} resulting in a θ value of 61° for the spectrum presented by Leskes et al,⁵⁹ a similar value (of 31.2°) far from the magic angle has been reported by Nishiyama et al. for the implementation of windowed $PMLG5_{mm}^{xx}$ at an MAS frequency of 80 kHz and a 1H nutation frequency of 125 kHz.⁵⁷ Moreover, the actual rotation, ξ_{LG_expt} , reported by Nishiyama et al. of 243° is similar to that of 239° for our implementation of both windowed $PMLG5_{mm}^{xx}$ and $PMLG9_{mm}^{xx}$ at a MAS frequency of 60 kHz (see **Table 1**). **Table 1** also lists the implementations of $PMLG5_{mm}^{xx}$ by Leskes et al. at 10 kHz MAS⁸⁵ and Mao & Pruski at 12.5, 19.5, 25.0 and 41.7 kHz MAS.⁹³ the angle θ is seen to vary between 45° and 64° . It is observed that an angle θ below and above the magic angle corresponds to an actual rotation, ξ_{LG_expt} , less than and more than the ideal 360° ,



respectively. For the good decoupling performance observed at $\nu_0 = 1$ GHz with windowed $PMLG5_{mm}^{\bar{x}x}$ for a ^1H nutation frequency of only 51 kHz (see **Fig. 3c**), where the angle θ is only 17.6° .

Table 1. Implementation of $PMLG5_{mm}^{\bar{x}x}$ and $PMLG9_{mm}^{\bar{x}x}$ ^1H homonuclear decoupling: variation from the ideal Lee-Goldburg condition for this work and previous publications

| Decoupling | ν_r (kHz) | ν_1 (kHz) | τ_{LG} (μ s) | τ_{LG_expt} (μ s) | θ_m (deg) | θ (deg) | $\Delta \nu_{LG}$ (kHz) | $\Delta \nu_{LG_expt}$ (kHz) | ν_{eff_LG} (kHz) | $\nu_{eff_LG_expt}$ (kHz) | ξ_{LG} (deg) | ξ_{LG_expt} (deg) |
|---|------------------|------------------|---------------------------|---------------------------------|---------------------|----------------|----------------------------|----------------------------------|--------------------------|--------------------------------|---------------------|---------------------------|
| Windowed $PMLG5^{\overline{x}x}_{mm}$ ^a (500 MHz) | 60.0 | 106 | 7.70 | 3.10 | 54.7 | 29.7 | 75.0 | 186.2 | 129.8 | 214.3 | 360.0 | 239.2 |
| Windowless $PMLG5^{\overline{x}x}_{mm}$ ^b (500 MHz) | 60.0 | 106 | 7.70 | 3.10 | | 29.7 | 75.0 | 186.2 | 129.8 | 214.3 | | 239.2 |
| Windowed $PMLG9^{\overline{x}x}_{mm}$ ^a (500 MHz) | 60.0 | 113 | 7.23 | 2.92 | | 29.7 | 79.9 | 197.7 | 138.4 | 227.7 | | 239.4 |
| Windowless $PMLG9^{\overline{x}x}_{mm}$ ^b (500 MHz) | 60.0 | 113 | 7.23 | 2.92 | | 29.7 | 79.9 | 197.7 | 138.4 | 227.7 | | 239.4 |
| Windowed $PMLG5^{\overline{x}x}_{mm}$ ^c (1 GHz, $\nu_1 = 108$ kHz) | 60.0 | 108 | 7.56 | 3.10 | | 30.1 | 76.4 | 186.2 | 132.3 | 215.3 | | 240.3 |
| Windowed $PMLG5^{\overline{x}x}_{mm}$ ^c (1 GHz, $\nu_1 = 51$ kHz) | 60.0 | 51 | 16.01 | 3.63 | | 17.6 | 36.1 | 159.3 | 62.4 | 167.2 | | 218.2 |
| Literature parameters | | | | | | | | | | | | |
| $PMLG5^{\overline{x}x}_{pp}$ ^d | 80.0 | 125 | 6.53 | 2.80 | 54.7 | 31.2 | 88.4 | 206.2 | 153.1 | 241.1 | 360.0 | 243.1 |
| $PMLG5^{\overline{x}x}_{mm}$ ^e | 65.0 | 216 | 3.78 | 4.80 | | 60.9 | 152.7 | 120.3 | 264.5 | 247.2 | | 427.2 |
| $PMLG5^{\overline{x}x}_{mm}$ ^f | 41.7 | 155 | 5.27 | 3.75 | | 45.2 | 109.6 | 154.0 | 189.8 | 218.5 | | 294.9 |
| $PMLG5^{\overline{x}x}_{mm}$ ^f | 41.7 | 155 | 5.27 | 7.75 | | 64.3 | 109.6 | 74.5 | 189.8 | 172.0 | | 479.8 |
| $PMLG5^{\overline{x}x}_{mm}$ ^g | 12.5 | 78 | 10.47 | 12.50 | | 59.4 | 55.2 | 46.2 | 95.5 | 90.6 | | 407.9 |
| $PMLG5^{\overline{x}x}_{mm}$ ^g | 19.5 | 126 | 6.48 | 8.00 | | 60.2 | 89.1 | 72.2 | 154.3 | 145.2 | | 418.2 |
| $PMLG5^{\overline{x}x}_{mm}$ ^g | 25.0 | 162 | 5.04 | 6.25 | | 60.3 | 114.6 | 92.4 | 198.4 | 186.5 | | 419.6 |
| $PMLG5^{\overline{x}x}_{mm}$ ^h | 10.0 | 95 | 8.59 | 7.25 | | 50.0 | 67.2 | 79.6 | 116.4 | 124.0 | | 323.5 |
| $PMLG5^{\overline{x}x}_{mm}$ ⁱ | 65.0 | 250 | 3.27 | 5.00 | | 65.2 | 176.8 | 115.5 | 306.2 | 275.4 | | 495.7 |

Parameters from this work for a) **Fig. 3b** and **Table 3**, b) **Fig. S3** and c) **Fig. 3c** and **Table 3**

Values extracted from d) Nishiyama et al. Fig. 2 and 3,⁵⁷ e) Leskes et al. Table 1,⁵⁹ f) and g) Mao et al.,⁹³ Fig. 3 and Fig. 2, respectively; h) Leskes et al. Fig. 2;⁸⁵ i) simulated values extracted from Leskes et al. Fig. 2⁸⁵

Table 2 states the τ_c values, as calculated from τ_{LG_expt} , τ_w and τ_{tilt} using eq. 10, for the implementations of $PMLG5_{mm}^{\bar{x}x}$ and $PMLG9_{mm}^{\bar{x}x}$ in this work, as well as that reported in the literature. An important parameter for predicting decoupling performance is the ratio, ψ , of the MAS rotor period, τ_r , to the decoupling cycle time, τ_c , and vice versa, the ratio of the corresponding frequency, $\nu_c = 1/\tau_c$, to the MAS frequency, ν_r .⁶⁵

$$\Psi = \frac{\tau_r}{\tau_c} = \frac{\nu_c}{\nu_r} \quad (11)$$



For low to moderate MAS frequencies, small integer values of ψ are to be avoided since these values correspond to recoupling rather than decoupling conditions.^{53,91,94-96} For fast MAS (of at least 40 kHz), there are more values of ψ that need to be avoided.^{62,65,93} Specifically, by employing bimodal Floquet theory, Leskes et al. have identified values of n and k that result in deteriorated decoupling due to zero-order and first-order recoupling conditions, according to:

$$n\nu_r + k\nu_c = 0, \quad (12)$$

where n takes values 1, 2, 3, 4 while $-15 \leq k \leq -1$.⁶⁵ While there is a dense set of degeneracies for values of ψ below 1.50, there are windows of good decoupling performance that can be found. The ψ value of both the windowless sequences, $PMLG5_{mm}^{\bar{x}x}$ ($\psi = 1.34$) and $PMLG9_{mm}^{\bar{x}x}$ ($\psi = 1.43$), are in line with the value of 1.40 – 1.60 reported by Mao et al. for spectra acquired among a range of different spinning frequencies (12.5 kHz to 41.7 kHz) and ^1H nutation frequencies (78 kHz – 162 kHz) as indicated in **Table 1** and **2**.⁹³ For windowed sequences, the ψ value is usually lower. For the 1D CRAMPS spectra presented in **Fig. 3b**, **Table 2** shows that ψ equals 0.58 and 0.57 for windowed $PMLG5_{mm}^{\bar{x}x}$ and windowed $PMLG9_{mm}^{\bar{x}x}$, respectively, at $\nu_0 = 500$ MHz, and 0.61 and 0.53 at $\nu_0 = 1$ GHz for a ^1H nutation frequency of 108 and 51 kHz, respectively. These ψ values are similar to the values of 0.60 and 0.63 for the experimental implementation of windowed $PMLG5_{mm}^{\bar{x}x}$ by Nishiyama et al. at an MAS frequency of 80 kHz and a ^1H nutation frequency of 125 kHz⁵⁷ and by Leskes et al. at an MAS frequency of 65 kHz and a ^1H nutation frequency of 216 kHz,⁵⁹ respectively.

Table 2. Implementation of $PMLG5_{mm}^{\bar{x}x}$ and $PMLG9_{mm}^{\bar{x}x}$ ^1H homonuclear decoupling: scaling factors and comparison of rotor period to cycle time for this work and previous publications

| | τ_{LG_expt} (μs) | τ_w (μs) | τ_{tilt} (μs) | τ_c (μs) | τ_r (μs) | ψ^l | λ_{CS_calc} | λ_{CS_expt} |
|--|-------------------------------------|----------------------------|---------------------------------|----------------------------|----------------------------|----------|----------------------|----------------------|
| Windowed $PMLG5_{mm}^{\bar{x}x}$ ^a (500 MHz) | 3.10 | 7.20 | 0.54 | 28.96 | 16.67 | 0.58 | 0.76 ^k | 0.82 |
| Windowless $PMLG5_{mm}^{\bar{x}x}$ ^b (500 MHz) | 3.10 | - | - | 12.40 | 16.67 | 1.34 | 0.76 ^j | 0.66 |
| Windowed $PMLG9_{mm}^{\bar{x}x}$ ^a (500 MHz) | 2.92 | 7.20 | 0.82 | 29.36 | 16.67 | 0.57 | 0.77 ^k | 0.76 |
| Windowless $PMLG9_{mm}^{\bar{x}x}$ ^b (500 MHz) | 2.92 | - | - | 11.68 | 16.67 | 1.43 | 0.78 ^j | 0.60 |
| Windowed $PMLG5_{mm}^{\bar{x}x}$ ^c (1 GHz, 108 kHz) | 3.10 | 7.20 | 0.18 | 27.52 | 16.67 | 0.61 | 0.74 ^k | 0.82 |
| Windowed $PMLG5_{mm}^{\bar{x}x}$ ^c (1 GHz, 51 kHz) | 3.63 | 7.20 | 0.70 | 31.70 | 16.67 | 0.53 | 0.90 ^k | 0.92 |



| Literature parameters | | | | | | | | |
|---|-------|------|---|-------|--------|------|-------------------|------|
| $PMLG5^{\overline{xx}}_{pp}$ ^d | 2.80 | 4.84 | - | 20.88 | 12.50 | 0.60 | 0.86 ^j | 0.82 |
| $PMLG5^{\overline{xx}}_{mm}$ ^e | 4.80 | 2.70 | - | 24.60 | 15.38 | 0.63 | 0.40 ^j | 0.48 |
| $PMLG5^{\overline{xx}}_{mm}$ ^f | 3.75 | - | - | 15.00 | 24.00 | 1.60 | 0.50 ^j | 0.36 |
| $PMLG5^{\overline{xx}}_{mm}$ ^f | 7.75 | - | - | 31.00 | 24.00 | 0.77 | 0.19 ^j | 0.21 |
| $PMLG5^{\overline{xx}}_{mm}$ ^g | 12.50 | - | - | 50.00 | 80.00 | 1.60 | 0.26 ^j | - |
| $PMLG5^{\overline{xx}}_{mm}$ ^g | 8.00 | - | - | 32.00 | 51.20 | 1.60 | 0.25 ^j | - |
| $PMLG5^{\overline{xx}}_{mm}$ ^g | 6.25 | - | - | 25.00 | 40.00 | 1.60 | 0.25 ^j | - |
| $PMLG5^{\overline{xx}}_{mm}$ ^h | 7.25 | 4.35 | - | 37.70 | 100.00 | 2.65 | 0.55 ^j | 0.47 |
| $PMLG5^{\overline{xx}}_{mm}$ ⁱ | 5.00 | - | - | 20.00 | 15.38 | 0.77 | 0.18 ^j | - |

View Article Online
DOI: 10.1039/D2CP01041K

Parameters from this work for a) **Fig. 3b** and **Table 3**, b) **Fig. S5** and c) **Fig. 3c** and **Table 3**

Values extracted from d) Nishiyama et al. Fig. 2 and 3,⁵⁷ e) Leskes et al. Table 1,⁵⁹ f) and g) Mao et al.,⁹³ Fig. 3 and Fig. 2, respectively; h) Leskes et al. Fig. 2;⁸⁵ i) simulated values extracted from Leskes et al. Fig. 2⁶⁵

λ_{CS} is calculated with j) eq. 15 and k) eq. 16 as stated in this paper, following from Nishiyama et al.⁵⁷

l) ψ is calculated with eq. 12, following from Leskes et al.⁶⁵

3.4 Windowed and windowless PMLG ^1H decoupling, ^1H spin-echo dephasing and scaling factors

It is well established that the application of rf ^1H homonuclear decoupling leads to a chemical shift scaling: for a static sample, the chemical shift scaling factor, λ_{CS} , for perfect decoupling cannot exceed $\cos^{-1}(\theta_m) = 1/\sqrt{3} = 0.577$.^{64,96,97} The 1D ^1H CRAMPS spectra presented in **Fig. 3b** and **Fig. 3c** have chemical shift axes that have been corrected for this scaling, i.e., a scaling is applied so as to ensure that the chemical shift separation between the NH_3^+ peak and the lower ppm CH_2 peak corresponds to the MAS-only ^1H chemical shifts, i.e., $8.4 - 3.0 = 5.4$ ppm. The full width at half maximum, (FWHM), of the three ^1H resonances before and after scaling for the spectra presented in **Fig. 3b** and **Fig. 3c** are presented in **Table 3**. **Table 3** also states that λ_{CS} equals 0.82 and 0.76 for windowed $PMLG5^{\overline{xx}}_{mm}$ and windowed $PMLG9^{\overline{xx}}_{mm}$, respectively, at $\nu_0 = 500$ MHz, and 0.82 and 0.92 at $\nu_0 = 1$ GHz for a ^1H nutation frequency of 108 and 51 kHz, respectively. **Table 3** also reports, as a measure of decoupling efficiency, K, given by

$$K = \frac{\text{FWHM}_{\text{MAS}} - \text{FWHM}_{\text{scaled}}}{\text{FWHM}_{\text{MAS}}} = \frac{\text{FWHM}_{\text{MAS}} - (\text{FWHM}_{\text{PMLG}}/\lambda_{CS})}{\text{FWHM}_{\text{MAS}}}, \quad (13)$$

where a K closer to 1 corresponds to better decoupling performance. FWHM_{MAS} is obtained under MAS alone, $\text{FWHM}_{\text{PMLG}}$ is the linewidth recorded using PMLG, and FWHM after scaling, $\text{FWHM}_{\text{scaled}}$, is equal to $\text{FWHM}_{\text{PMLG}}/\lambda_{CS}$. High scaling factors that are significantly above 0.577, like those stated in **Table 3**, have been reported for 60 kHz MAS by Salager et al. for an experimental optimisation protocol based on a quality factor considering the intensity of the two most intense resonances, CH_3 and NH_3 , in β -AspAla as well as their peak separation in Hz.⁵⁸ Specifically, λ_{CS} equals 0.73 and 0.84 for the eDUMBO-PLUS-1 and eDUMBO-PLUS-large sequences, respectively, for 60 kHz MAS and a ^1H nutation frequency of 170 kHz, with optimum resolution observed for eDUMBO-PLUS-1. Salager et al. have further presented a scaling factor



theorem for homonuclear decoupling, derived for a static system of homonuclear $I = 1/2$ spins coupled by a dipolar interaction that are subject to cyclic rf irradiation:

$$|\lambda_{\text{CS}}|^2 \leq \frac{1}{3}(2|\lambda_{\text{D}}| + 1), \quad (14)$$

where λ_{D} is the dipolar scaling factor, i.e., zero corresponds to perfect decoupling, showing that λ_{CS} cannot exceed $1/\sqrt{3}$, when $\lambda_{\text{D}} = 0$.⁶⁴

For $PMLG5_{mm}^{\bar{x}x}$, Nishiyama et al. report a λ_{CS} of 0.82 at 80 kHz MAS and a ^1H nutation frequency of 125 kHz.

Nishiyama et al. further state equations for calculating λ_{CS} for $PMLG5_{mm}^{\bar{x}x}$ decoupling without and with tilt pulses:

$$\lambda_{\text{CS_calc_no_tilt_pulses}} = \frac{2\tau_{\text{LG_expt}} \cos^2 \theta + \tau_{\text{w}}}{2\tau_{\text{LG_expt}} + 2\tau_{\text{tilt}} + \tau_{\text{w}}}, \quad (15)$$

$$\lambda_{\text{CS_calc_with_tilt_pulses}} = \frac{\frac{2\tau_{\text{th}} \sin \theta}{\theta} + 2\tau_{\text{LG_expt}} \cos \theta \cos 2\theta + \tau_{\text{w}}}{2\tau_{\text{LG_expt}} + 2\tau_{\text{tilt}} + \tau_{\text{w}}}. \quad (16)$$

These calculated λ_{CS} values are presented in **Table 2** for the experimental implementations of $PMLG5_{mm}^{\bar{x}x}$ in the literature, as well as $PMLG5_{mm}^{\bar{x}x}$ and $PMLG9_{mm}^{\bar{x}x}$ in this work. Deviation of the experimental scaling factor compared to theoretical behaviour can arise from phase transients that cause phase propagation delays.^{91,98}



Table 3. Analysis of windowed $PMLG5_{mm}^{\overline{xx}}$ and $PMLG9_{mm}^{\overline{xx}}$ ^1H homonuclear decoupling efficiency for ^1H ($\nu_0 = 500$ MHz and 1 GHz) CRAMPS NMR at $\nu_r = 60$ kHz of ^{15}N -glycine^a

| | δ (ppm) | FWHM _{MAS} (Hz) | FWHM _{MAS} (ppm) | FWHM _{PML} _G (Hz) | FWHM _{PML} _G (ppm) | FWHM _{scale} _d (Hz) | FWHM _{scale} _d (ppm) | Scaling factor, λ_{CS} | K ^b | FWHM _{PML} _G (Hz) | FWHM _{PML} _G (ppm) | FWHM _{scale} _d (Hz) | FWHM _{scale} _d (ppm) | Scaling factor, λ_{CS} | K ^b |
|------------------------------|----------------|--------------------------|---------------------------|---|--|---|--|---------------------------------------|----------------|---|--|---|--|---------------------------------------|----------------|
| $\nu_0 = 500$ MHz | | | | $PMLG5^{\overline{xx}}_{mm}$ ($\nu_1 = 106$ kHz) | | | | | | $PMLG9^{\overline{xx}}_{mm}$ ($\nu_1 = 113$ kHz) | | | | | |
| NH ₃ ⁺ | 8.4 | 664 | 1.33 | 230 | 0.46 | 280 | 0.56 | 0.82 | 0.58 | 273 | 0.55 | 359 | 0.72 | 0.76 | 0.46 |
| CH ₂ | 4.2 | 800 ^c | 1.60 | 217 | 0.43 | 264 | 0.53 | | 0.67 | 213 | 0.43 | 280 | 0.56 | | 0.65 |
| CH ₂ | 3.0 | 800 ^c | 1.60 | 224 | 0.45 | 273 | 0.55 | | 0.66 | 232 | 0.46 | 305 | 0.61 | | 0.62 |
| $\nu_0 = 1$ GHz | | | | $PMLG5^{\overline{xx}}_{mm}$ ($\nu_1 = 108$ kHz) | | | | | | $PMLG5^{\overline{xx}}_{mm}$ ($\nu_1 = 51$ kHz) | | | | | |
| NH ₃ ⁺ | 8.4 | 700 | 0.70 | 583 | 0.58 | 711 | 0.71 | 0.82 | −0.02 | 475 | 0.48 | 516 | 0.52 | 0.92 | 0.26 |
| CH ₂ | 4.2 | 740 | 0.74 | 346 | 0.35 | 422 | 0.42 | | 0.43 | 448 | 0.45 | 487 | 0.49 | | 0.34 |
| CH ₂ | 3.0 | 740 | 0.74 | 311 | 0.31 | 379 | 0.38 | | 0.49 | 440 | 0.44 | 478 | 0.48 | | 0.35 |

^a See spectra in **Fig. 3b** ($\nu_0 = 500$ MHz) and **Fig. 3c** ($\nu_0 = 1$ GHz), for the pulse sequence in **Fig. 2b** and experimental parameters in **Table 2**^b calculated with **eq. 13**

As well as scaling the chemical shifts, ^1H homonuclear decoupling also scales evolution under a heteronuclear J -coupling by the same factor.^{37,57,79} For magnetisation transfer from ^{15}N to ^1H during the spin echoes of the refocused INEPT pulse sequence element, the efficiency depends upon this scaling of the ^{15}N - ^1H J -couplings, but also the spin-echo dephasing time, T_2' .^{93,99,100}

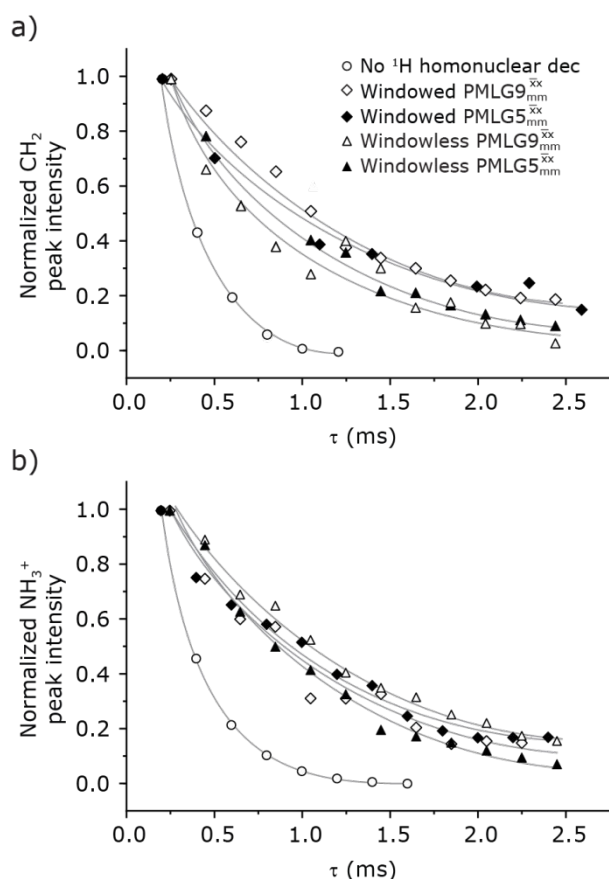


Figure 4. Dephasing of the ^{15}N -glycine a) CH_2 (the higher ppm ^1H resonance is considered) and b) NH_3^+ proton resonances as a function of the spin-echo (see **Fig. 2c**) duration, τ , with no ^1H homonuclear decoupling (empty circles), windowed PMLG9^{xx} (empty diamonds), windowed PMLG5^{xx} (full diamonds), windowless PMLG9^{xx} (empty triangles), and windowless PMLG5^{xx} (full triangles) for nutation frequencies and resonance offsets as stated in **Table 4**. Fits to an exponential decay function are shown, with the spin-echo dephasing times, T_2' , as listed in **Table 4**. 16 transients were co-added for a recycle delay of 3 s. For all experiments with windowed ^1H homonuclear decoupling, $\tau_w = 7.20 \mu\text{s}$.

Fig. 4 compares spin-echo dephasing curves (see pulse sequence in **Fig. 2c**) for MAS alone to those for windowed and windowless PMLG5^{xx} and PMLG9^{xx} , with the values for experimental parameters and extracted T_2' presented in **Table 4**. (Note that PMLG9^{xx} homonuclear decoupling was implemented with a slightly changed nutation frequency of $\nu_1 = 109 \text{ kHz}$, as compared to $\nu_1 = 113 \text{ kHz}$ for the 1D CRAMPS spectrum in **Fig. 3b**). In windowless PMLG decoupling, there is continuous rf irradiation, i.e., there are no



tilt pulses and $\tau_w = 0$, while, in the windowed version, τ_w is replaced by a delay (**Fig. 2e**). Note that the first implementation of PMLG was in the indirect dimension of a two-dimensional ^1H - ^1H experiment where there is evolution under MAS alone in the direct dimension.⁴⁹ Such a 2D experiment (see **Fig. 2d**) is used to measure λ_{CS} for our implementation of windowless $\text{PMLG}5_{\text{mm}}^{\text{xx}}$ and $\text{PMLG}9_{\text{mm}}^{\text{xx}}$, as reported in **Tables 2** and **4** (spectra are presented in **Fig. S4**).

Table 4 ^1H dephasing time, T_2' , and T_2' scaled by the experimental λ_{CS} , $\lambda_{\text{CS}} T_2'$, as determined by a ^1H spin-echo MAS NMR experiment^a for ^{15}N -glycine with optimised rf carrier offset and ν_1

| | Offset (kHz) | ν_1 (kHz) | λ_{CS} | $\text{NH}_3^+ T_2'$ (ms) | $\text{NH}_3^+ \lambda_{\text{CS}} T_2'$ (ms) | $\text{CH}_2 T_2'^b$ (ms) | $\text{CH}_2 \lambda_{\text{CS}} T_2'$ (ms) |
|---|--------------|---------------|-----------------------|---------------------------|---|---------------------------|---|
| No decoupling | 2 | - | 1 | 0.25 | 0.25 | 0.22 | 0.22 |
| Windowed $\text{PMLG}5_{\text{mm}}^{\text{xx}}$ | 1 | 106 | 0.82 | 1.04 | 0.85 | 1.14 | 0.93 |
| Windowed $\text{PMLG}9_{\text{mm}}^{\text{xx}}$ | 0.75 | 109 | 0.76 | 0.91 | 0.69 | 1.10 | 0.84 |
| Windowless $\text{PMLG}5_{\text{mm}}^{\text{xx}}$ | 1 | 106 | 0.66 | 0.86 | 0.57 | 0.80 | 0.53 |
| Windowless $\text{PMLG}9_{\text{mm}}^{\text{xx}}$ | -0.25 | 109 | 0.60 | 1.15 | 0.69 | 0.78 | 0.47 |

^a As implemented at $\nu_0 = 500$ MHz and $\nu_1 = 60$ kHz, see **Fig. 4a** for the CH_2 resonance and **Fig. 4b** for the NH_3^+ peak. τ_{tilt} is equal to $0.54 \mu\text{s}$ for windowed $\text{PMLG}5_{\text{mm}}^{\text{xx}}$ and $0.82 \mu\text{s}$ for windowed $\text{PMLG}9_{\text{mm}}^{\text{xx}}$

^b For the CH_2 group, the T_2' of the higher-ppm ^1H resonance is stated

Considering **Fig. 4** and **Table 4**, the ^1H dephasing times, T_2' , for the CH_2 (the higher ppm resonance is considered) and NH_3^+ peaks are 0.22 ms and 0.25 ms for 60 kHz MAS alone. With ^1H homonuclear decoupling the ^1H dephasing time for both groups increases. The longest CH_2 dephasing time is observed for windowed $\text{PMLG}5_{\text{mm}}^{\text{xx}}$, $T_2' = 1.14$ ms, slightly longer than for windowed $\text{PMLG}9_{\text{mm}}^{\text{xx}}$, where T_2' is equal to 1.10 ms. However, the scaling by λ_{CS} needs to be considered and **Table 4** reports the product of λ_{CS} and T_2' in each case. After this scaling (**Table 4**), windowed $\text{PMLG}5_{\text{mm}}^{\text{xx}}$ achieves an over 4 fold improvement with respect of MAS alone, compared to the slightly under 4 fold improvement of windowed $\text{PMLG}9_{\text{mm}}^{\text{xx}}$. A similar comparison can be made for the NH_3^+ peak, where windowless $\text{PMLG}9_{\text{mm}}^{\text{xx}}$ shows the longest T_2' equal to 1.15 ms and the longest value of the product, $\lambda_{\text{CS}} T_2'$ of 0.69 ms, thanks again to the large λ_{CS} ; this corresponds to a just under 3 fold improvement with respect to MAS alone.

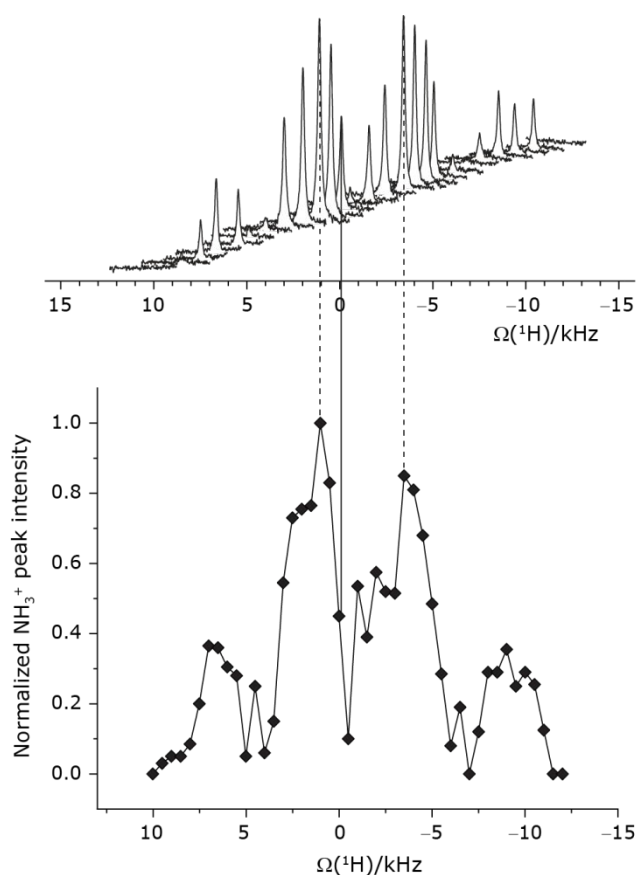


3.5 Optimisation of the ^{15}N -glycine NH_3^+ signal intensity in a 1D-filtered CP-refocused INEPT NMR spectrum for PMLG ^1H decoupling at 60 kHz MAS

Under a ^1H homonuclear decoupling sequence such as PMLG, the proton offset frequency influences the performance;^{53,92} this is linked to the overall z-rotation that the spins need under decoupling to avoid artifacts and RF imperfections.⁸⁵ As shown by Leskes et al.,⁸⁹ the non-supercycled m -block is particularly beneficial in narrowing lines of strong coupled spins, as for the CH_2 groups of ^{15}N -glycine, close to the on-resonance position. With the implementation of supercycled PMLG schemes,⁹⁰ the sign of the offset is no longer a determining factor as the supercycle brings the effective rotation of the spins closer to the z-axis.¹⁰¹ However, the choice of the optimum offset still plays a significant role for achieving good decoupling performance, therefore it is necessary to investigate both positive and negative offsets. Here the optimization was performed directly on the ^{15}N - ^1H CP-Refocused INEPT experiment, where windowed $\text{PMLG}5_{mm}^{\text{xx}}$ was applied over a wide range of offset values from $\sim +10$ kHz to -12 kHz, whereby on-resonance corresponds to the NH_3^+ peak. **Figure 5** shows that the best offsets in term of sensitivity are at $+1$ kHz and -3.5 kHz, highlighted by dashed vertical lines. Between the two best performing offsets, the sensitivity experiences a fluctuation (**Fig. 5**) corresponding to the on-resonance position (solid line), dropping to zero for a small negative offset of -0.5 kHz. It is then important to optimize the offset avoiding the on-resonance position. The need for a fine optimization of this parameter is emphasized by the considerable change in sensitivity that is observed for a small variation of the offset.^{53,54,96} For example, the relative sensitivity of the NH_3^+ peak falls from over 0.8 to 0.5 when switching the offset from ~ -3.5 to -2.5 kHz. In general, in **Figure 5** the offsets close to the on-resonance position yield better sensitivity symmetrically in a range between ± 4 kHz, in agreement with the rotation improvement brought by the supercycled ^1H homonuclear decoupling.⁸⁹

The same offset optimization was carried out on the different PMLG-block types, and similar trends were shown with a better sensitivity in the proximity of the on-resonance position. As stated in Table 4, the offsets which gave the maximum sensitivity were 0.75 kHz for windowed $\text{PMLG}9_{mm}^{\text{xx}}$, -0.25 kHz for $\text{PMLG}9_{mm}^{\text{xx}}$ and $+1$ kHz for $\text{PMLG}5_{mm}^{\text{xx}}$ (the same as windowed $\text{PMLG}5_{mm}^{\text{xx}}$) (See **Fig. S5**).





View Article Online
DOI: 10.1039/D2CP01041K

Figure 5. ^1H RF carrier optimization for a 1D-filtered ($t_1 = 0$) ^{15}N - ^1H ($\nu_0 = 500$ MHz) CP (contact time = 2 ms)-Refocused INEPT MAS ($\nu_r = 60$ kHz) NMR experiment for ^{15}N -labelled glycine, whereby windowed $PMLG5_{mm}^{\overline{xx}}$ ^1H homonuclear decoupling was applied with $\tau_{LG_expt} = 3.1 \mu\text{s}$, $\tau_{tilt} = 0.54 \mu\text{s}$ and a ^1H nutation frequency, ν_1 , of 106 kHz during τ_1 (1.999 ms, $69 \tau_c$) and 104 kHz during τ_2 (1.391 ms, $48 \tau_c$). 16 transients were coadded. For all experiments with windowed ^1H homonuclear decoupling, $\tau_w = 7.20 \mu\text{s}$. The zero-offset is set with the carrier being on resonance with the NH_3^+ peak, corresponding to the solid vertical line. Dashed vertical lines indicate the two highest signal intensities at +1 kHz and -3.5 kHz.

The implementation of the ^1H decoupling scheme into the heteronuclear correlation experiment required the further optimisation of the spin-echo durations during the Refocused INEPT transfer. This was carried out separately for τ_1 and τ_2 (see pulse sequence in **Fig. 1a**) because, as stated in section 3.1, for the two spin echoes, different spins are along the transverse plane, ^{15}N for the first and ^1H for the second spin echo. To ensure the best conditions, a double-optimisation of ^1H homonuclear decoupling nutation frequency vs τ_1 and τ_2 was carried out. Specifically, the two-variable optimisation was performed for ^{15}N -labelled glycine for windowed or windowless $PMLG5_{mm}^{\overline{xx}}$ and $PMLG9_{mm}^{\overline{xx}}$ for the best offset (see **Table 5**) and the results are reported in **Table 5**. The dependence with respect to the second spin-echo duration, τ_2 , is presented in **Figure 6**. Note from eq 2, a sine dependence is expected from which the scaled J coupling could be extracted.



Table 5 Optimised τ_f carrier offset, spin-echo duration and nutation frequencies for four implementations of PMLG ^1H homonuclear decoupling and MAS-alone for a ^{15}N - ^1H CP-refocused INEPT MAS NMR experiment for ^{15}N -glycine^a

| ^1H homonuclear decoupling | Offset (kHz) ^b | λ_{CS} | τ_1 (ms) ^c | $\lambda_{\text{CS}} \tau_1$ (ms) | ν_1 (kHz) for τ_1 | τ_2 (ms) ^c | $\lambda_{\text{CS}} \tau_2$ (ms) | ν_1 (kHz) for τ_2 | Relative intensity ^d |
|--|---------------------------|-----------------------|----------------------------|-----------------------------------|----------------------------|----------------------------|-----------------------------------|----------------------------|---------------------------------|
| No decoupling | 2.00 | 1.00 | 1.600 | 1.600 | - | 0.300 | 0.300 | - | 0.08 |
| Windowed $\text{PMLG}5_{mm}^{\text{xx}}$ | 1.00 | 0.82 | 1.999 (69 τ_c) | 1.639 | 106 | 1.391 (48 τ_c) | 1.140 | 106 | 1.00 |
| Windowed $\text{PMLG}9_{mm}^{\text{xx}}$ | 0.75 | 0.76 | 2.085 (71 τ_c) | 1.585 | 104 | 1.498 (51 τ_c) | 1.138 | 106 | 0.80 |
| Windowless $\text{PMLG}5_{mm}^{\text{xx}}$ | 1.00 | 0.66 | 2.096 (169 τ_c) | 1.383 | 102 | 0.496 (40 τ_c) | 0.327 | 102 | 0.52 |
| Windowless $\text{PMLG}9_{mm}^{\text{xx}}$ | -0.25 | 0.60 | 2.091 (179 τ_c) | 1.254 | 104 | 1.192 (102 τ_c) | 0.715 | 102 | 0.48 |

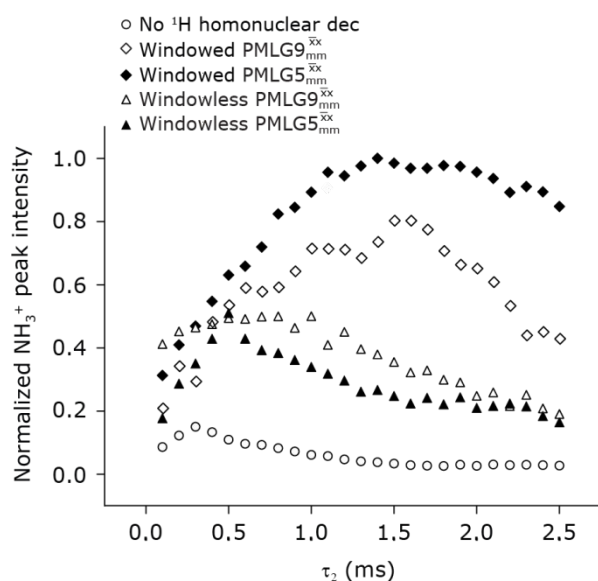
^a As implemented on at $\nu_0 = 500$ MHz and $\nu_f = 60$ kHz. τ_{tilt} is equal to 0.54 μs for windowed $\text{PMLG}5_{mm}^{\text{xx}}$ and 0.82 μs for windowed $\text{PMLG}9_{mm}^{\text{xx}}$.

See Fig. 6

^b relative to the $\text{NH}_3^+ ^1\text{H}$ resonance^c $\tau_1 = n \tau_c$, $\tau_2 = m \tau_c$, where n and m are positive integers^d See Fig. 7

Considering Table 5, the ^1H nutation frequencies are in the range of 102-106 kHz for all the PMLG-block types, with a maximum of 2 kHz difference between that applied in τ_1 and τ_2 for the same PMLG block. For τ_1 , the optimum values for PMLG decoupling are 2.0 or 2.1 ms, as compared to 1.6 ms from MAS alone. However, as discussed in section 3.4, it is the product $\lambda_{\text{CS}} \cdot \tau$, that needs to be considered, in which case similar values are obtained as compared to MAS alone. By comparison, a clear difference is observed for τ_2 , where the evolution of ^1H coherence is markedly affected by the ^1H - ^1H dipolar couplings. Indeed, the coherence transfer increases from 0.3 ms for MAS alone to 1.5 ms for windowed $\text{PMLG}9_{mm}^{\text{xx}}$ and 1.4 ms for windowed $\text{PMLG}5_{mm}^{\text{xx}}$. After scaling, the product $\lambda_{\text{CS}} \tau_2$, 1.14 ms for both windowed $\text{PMLG}9_{mm}^{\text{xx}}$ and $\text{PMLG}5_{mm}^{\text{xx}}$, are still ~ 4 times longer than the optimum τ_2 for MAS alone. We note a discrepancy for τ_2 under windowless $\text{PMLG}5_{mm}^{\text{xx}}$, which is considerably shorter (0.3 ms after scaling) with respect to the other ^1H homonuclear implementations.





View Article Online
DOI: 10.1039/D2CP01041K

Figure 6. Dependence upon the second spin-echo duration, τ_2 , for ^{15}N -labelled glycine of the NH_3^+ peak in a 1D-filtered ($t_1 = 0$) ^{15}N - ^1H ($\nu_0 = 500$ MHz) CP (contact time = 2 ms)-Refocused INEPT MAS ($\nu_r = 60$ kHz) NMR spectrum for: windowed $PMLG5^{\text{xx}}_{\text{mm}}$ ($\tau_{\text{LG_expt}} = 3.1$ μs , $\tau_{\text{tilt}} = 0.54$ μs , $\nu_1 = 106$ kHz for τ_1 and 106 kHz for τ_2 full diamonds), windowless $PMLG5^{\text{xx}}$ same conditions but with no tilt pulses, full triangles, with $\nu_1 = 102$ kHz for τ_1 and 102 kHz for τ_2), windowed $PMLG9^{\text{xx}}_{\text{mm}}$ ($\tau_{\text{LG_expt}} = 2.92$ μs , $\tau_{\text{tilt}} = 0.82$ μs , $\nu_1 = 104$ kHz for τ_1 and 106 kHz for τ_2 empty diamonds), windowless $PMLG9^{\text{xx}}$ same conditions but with no tilt pulses, empty triangles, with $\nu_1 = 104$ kHz for τ_1 and 102 kHz for τ_2), MAS alone (empty circles). 8 transients were coadded. For all experiments with windowed PMLG, $\tau_w = 7.20$ μs .

In **Figure 7**, we compare the different peak intensities for the NH_3^+ peak of ^{15}N -labelled glycine for the windowless and windowed implementation of $PMLG5^{\text{xx}}_{\text{mm}}$ and $PMLG9^{\text{xx}}_{\text{mm}}$ in a ^{15}N - ^1H CP-refocused INEPT 1D filtered ($t_1 = 0$) spectrum. The best performance is for our optimum implementation of windowed $PMLG5^{\text{xx}}_{\text{mm}}$ with a 12.5 times better relative sensitivity compared to MAS alone.

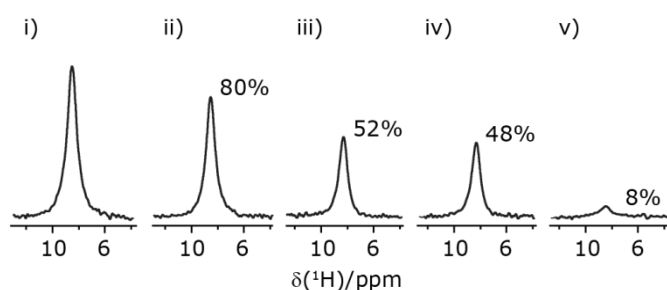


Figure 7. Comparison of the sensitivity of 1D-filtered ($t_1 = 0$) ^{15}N - ^1H ($\nu_0 = 500$ MHz) CP (contact time = 2 ms)-Refocused INEPT MAS ($\nu_r = 60$ kHz) NMR spectra of ^{15}N -glycine recorded with the application of different optimised PMLG ^1H decoupling conditions, i) to iv) compared to MAS alone, v): i) windowed $PMLG5^{\text{xx}}_{\text{mm}}$ ($\tau_{\text{LG_expt}} = 3.1$ μs , $\tau_{\text{tilt}} = 0.54$ μs , $\tau_1 = 1.999$ ms (69 τ_c) with $\nu_1 = 106$ kHz; $\tau_2 = 1.391$ ms (48 τ_c) with $\nu_1 = 106$ kHz), ii) windowed $PMLG9^{\text{xx}}_{\text{mm}}$ ($\tau_{\text{LG_expt}} = 2.92$ μs , $\tau_{\text{tilt}} = 0.82$ μs , $\tau_1 = 2.085$ ms (71 τ_c) with $\nu_1 = 104$ kHz; $\tau_2 = 1.498$ ms (51 τ_c) with $\nu_1 = 106$ kHz), iii) windowless $PMLG5^{\text{xx}}_{\text{mm}}$ ($\tau_{\text{LG_expt}} = 3.1$ μs , $\tau_1 = 2.096$ ms (169 τ_c) with $\nu_1 = 102$ kHz; $\tau_2 = 0.496$ ms (40 τ_c) with $\nu_1 = 102$ kHz), iv)



windowless $PMLG9_{mm}^{xx}$ ($\tau_{LG_expt} = 2.92 \mu s$, $\tau_1 = 2.090 ms$ ($179 \tau_c$) with $\nu_1 = 104 kHz$; $\tau_2 = 1.192 ms$ ($102 \tau_c$) with $\nu_2 = 102 kHz$), v) no decoupling $\tau_1 = 1.6 ms$ ($96 \tau_r$) and $\tau_2 = 0.3 ms$ ($18 \tau_r$). For all experiments with windowed 1H homonuclear decoupling, $\tau_w = 7.20 \mu s$. All the spectra were acquired with 16 coadded transients and the corresponding 1H transmitter offset reported in **Table 5**.

Finally, in this section, we compare the sensitivity and selectivity of the CP refocused INEPT experiment to that of a hNH double CP experiment. Specifically, the right-hand side of Figure 8 compares 1D-filtered MAS NMR spectra of ^{15}N -glycine recorded using the CP refocused INEPT experiment (red) or a hNH double CP experiment with a back (^{15}N to 1H) CP contact time of $200 \mu s$ (blue). In both cases, the 1H to ^{15}N CP contact time is $3.7 ms$, i.e., CP is used initially to efficiently generate ^{15}N transverse magnetisation. While the sensitivity of the CP refocused INEPT spectrum is half that of the double CP experiment, there is no intensity for the CH_2 1H resonances. Figure 8 also shows, for the double CP experiment, the dependence on the back (^{15}N to 1H) CP contact time, with a plateau in intensity reached after $200 \mu s$, though note that CH_2 1H resonance signal is already evident from $100 \mu s$.

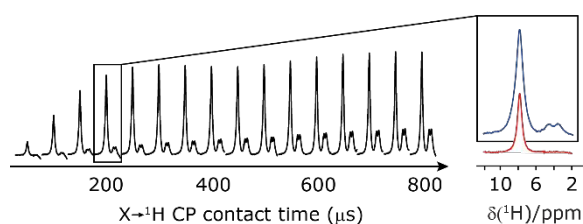


Figure 8. Comparison of the sensitivity of 1D-filtered ($t_1 = 0$) ^{15}N - 1H ($\nu_0 = 600 MHz$) MAS ($\nu_r = 60 kHz$) NMR spectra of ^{15}N -glycine recorded with a double CP experiment (blue) or a CP-refocused INEPT experiment (red). The build-up for the double CP experiment as a function of the ^{15}N to 1H CP contact time is also shown. In both cases, the 1H to ^{15}N CP contact time is $3.7 ms$. For refocused INEPT ^{15}N to 1H transfer, windowed $PMLG5_{mm}^{xx}$ ($\tau_{LG_expt} = 3.19 \mu s$, $\tau_{tilt} = 0.5 \mu s$ and $\tau_w = 7.20 \mu s$) is applied at a nutation frequency of $106 kHz$ for $\tau_1 = 2.334 ms$ ($140 \tau_r$) and $\tau_2 = 1.401 ms$ ($84 \tau_r$). All the spectra were acquired with 16 co-added transients and a 1H transmitter offset of $-4 kHz$.

3.6 2D ^{15}N - 1H CP-refocused INEPT NMR spectra with PMLG 1H decoupling at $60 kHz$ MAS of a dipeptide and a pharmaceutical at natural abundance

Due to the better sensitivity of windowed $PMLG5_{mm}^{xx}$ observed for glycine, it was selected as the 1H homonuclear decoupling sequence for a ^{15}N - 1H correlation experiment recorded for the β -AspAla dipeptide at natural isotopic abundance, with the improvement of resolution achieved in the 1D 1H CRAMPS compared here with a 1H one-pulse recorded at Larmor frequency of $500 MHz$ and $1 GHz$ (**Fig. 9a**). Note that a ^{15}N CP MAS spectrum for the β -AspAla dipeptide has been presented in Tatton *et al.*²² The ^{15}N - 1H CP-Refocused INEPT experiment was implemented with the offset and coherence transfer delays optimised for ^{15}N -labelled glycine, as stated in **Table 5**, i.e., $\tau_{LG_expt} = 3.1 \mu s$, $\tau_{tilt} = 0.54 \mu s$, $\tau_1 = 2.0 ms$ with $\nu_1 = 106 kHz$, ν_2



= 1.4 ms with $\nu_1 = 106$ kHz, and an offset of +1 kHz. High-performance ^1H homonuclear decoupling achieved with a finely optimised implementation of windowed $PMLG5_{mm}^{\overline{xx}}$ enables the recording at natural abundance of a 2D ^{15}N - ^1H correlation spectrum at 60 kHz MAS with a through-bond back transfer (**Fig. 9b**). The sensitivity of the windowed $PMLG5_{mm}^{\overline{xx}}$ implementation is compared to a ^{15}N - ^1H CP-Refocused INEPT spectrum recorded with no decoupling at the optimum $\tau_1 = 1.6$ ms and $\tau_2 = 0.3$ ms values in **Table 5** for ^{15}N -labelled glycine, only noise is observed in **Fig. 9c**.

As noted in section 3.1, there is a different dependence on the duration of the first spin echo, τ_1 , for a NH and NH_3^+ moiety, compare eqs 1 and 2. This is evident from Fig. 10 that shows the build-up of intensity in a 1D-filtered ^{15}N - ^1H CP-Refocused INEPT spectrum of the dipeptide β -AspAla. Two peaks are resolved for the higher-ppm NH and the lower-ppm NH_3^+ resonances (see deconvolution in Figure 10b), and it is evident maximum intensity is reached at a shorter spin-echo duration for the lower-ppm NH_3^+ peak at ~ 2.1 ms as compared to ~ 3.5 ms for the higher-ppm NH peak. As shown in Figure S7 of the Supporting Information, this is expected as based from a consideration of eq. 1 and eq. 2. Such an experiment could hence be used to distinguish different NH_x moieties, as for example has been demonstrated analogously for SiH_x groups.⁸²⁻⁸⁴

Furthermore, windowed $PMLG5_{mm}^{\overline{xx}}$ was employed to record a 2D ^{15}N - ^1H CP-Refocused INEPT spectrum of the pharmaceutical cimetidine at natural abundance (**Fig. 9d**), for which ^1H , ^{15}N CPMAS and ^{14}N - ^1H spectra have been presented in Refs. ^{102,103}. (For comparison, note that in Ref. 102, Tatton et al use a simple ^{15}N - ^1H heteronuclear spin echo with ^1H homonuclear decoupling to demonstrate spectral editing.) In this case, spin-echo curves were recorded, because, as discussed above, the optimum τ_1 and τ_2 durations in the Refocused INEPT pulse sequence element depends both on the J -coupling between the involved nuclei and the ^1H dephasing T_2' . The ^1H coherence lifetime (see **Fig. S6** and **Table S1** in comparison to Table 4) for two of the protons directly bonded to the nitrogens, N3 and N10, is longer than the NH_3^+ T_2' of ^{15}N -glycine acquired with the same windowed $PMLG5_{mm}^{\overline{xx}}$ ^1H decoupling. In addition, considering the above discussion of Fig. 10 and eqs 1 and 2, note that for a NH group, a maximum signal is observed at a longer τ_1 as compared to a NH_3^+ group. For this reason, τ_1 and τ_2 were increased to 2.5 ms and 2.0 ms, respectively. Note that weaker intensity is observed for the proton directly bonded to N15, where the respective ^1H T_2' is ~ 0.5 ms after scaling (**Table S1**). Further investigation is required to understand the shorter T_2' for this proton and the very weak signal for the N15-H15 cross peak in the 2D CP-refocused INEPT spectrum in Fig. 9d.



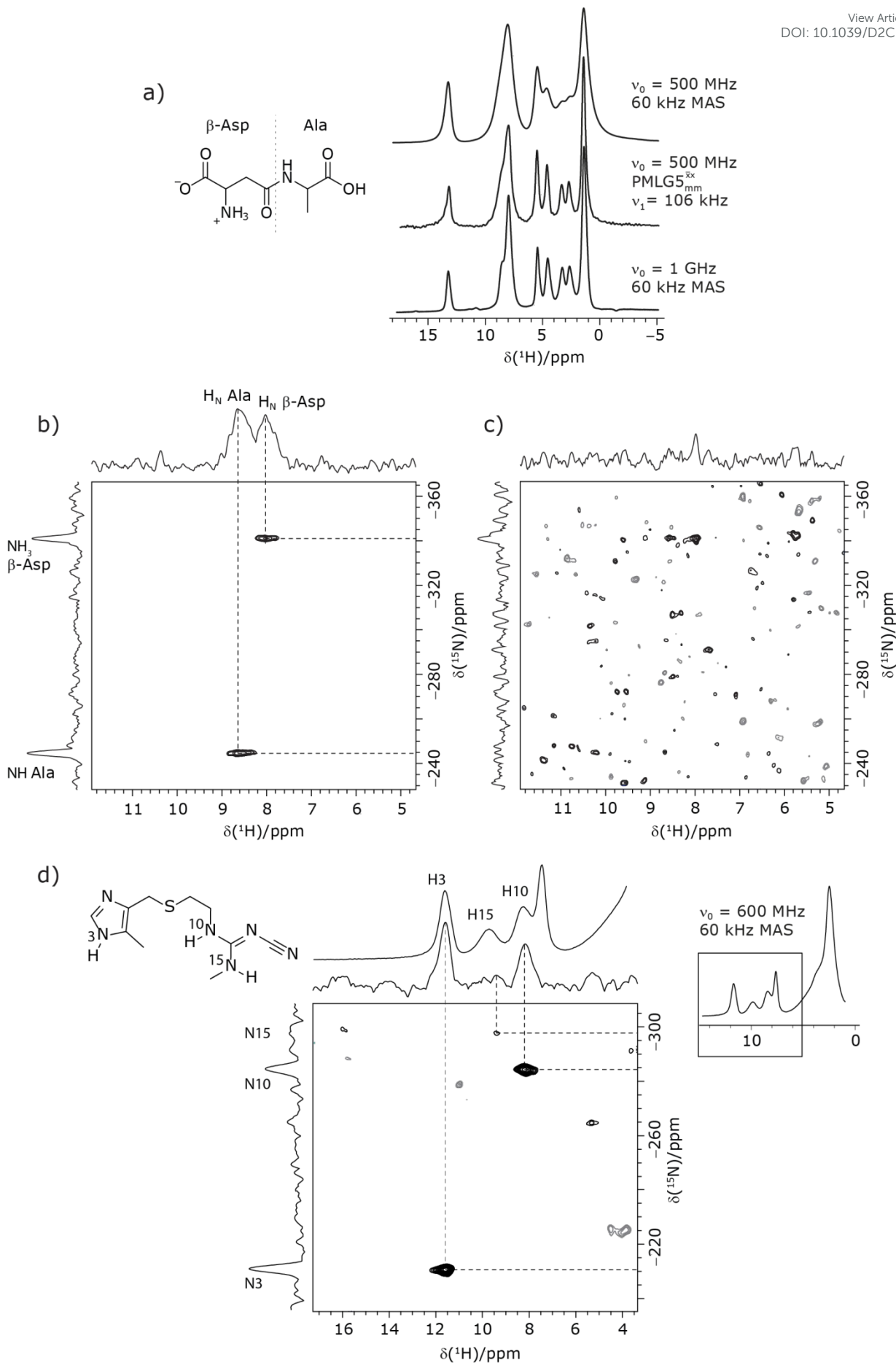


Figure 9. MAS ($\nu_r = 60$ kHz) NMR spectra of (a-c) the dipeptide β -AspAla and (d) the pharmaceutical cimetidine, in both cases at natural isotopic abundance, employing windowed $PMLG5_{mm}^{xx}$ ($\tau_{LG_expt} = 3.1 \mu s$, $\tau_{tilt} = 0.54 \mu s$ and $\tau_w = 7.20 \mu s$).

(a) Comparison of a 1H 1D CRAMPS spectrum acquired with windowed $PMLG5_{mm}^{xx}$ (at $\nu_0 = 500$ MHz, with 1H one-pulse spectra recorded at $\nu_0 = 500$ MHz and 1 GHz. (b, c) 2D ^{15}N - 1H ($\nu_0 = 500$ MHz) CP (contact time = 2 ms)-Refocused INEPT MAS NMR spectra with (b) windowed $PMLG5_{mm}^{xx}$ 1H homonuclear decoupling during the spin-echo durations used for ^{15}N - 1H Refocused INEPT coherence transfer or (c) MAS alone. In (b), windowed $PMLG5_{mm}^{xx}$ was implemented with $\nu_1(^1H) = 106$ kHz during τ_1 (1.999 ms, 69 τ_c) and $\nu_1(^1H) = 106$ kHz during τ_2 (1.391 ms, 48 τ_c), with the transmitter frequency centred at 10.3 ppm. For both b) and c), 224 transients were co-added for each of 96 t_1 FIDs, corresponding to a total experimental time of 23 h with a recycle delay of 3 s. The base contour is at 50 % of the respective maximum intensity in b) and c). d) A 2D ^{15}N - 1H ($\nu_0 = 600$ MHz) CP (contact time = 4 ms)-Refocused INEPT MAS NMR spectrum with windowed $PMLG5_{mm}^{xx}$ 1H homonuclear decoupling ($\nu_1(^1H) = 106$ kHz during τ_1 (2.491 ms, 86 τ_c) and $\nu_1(^1H) = 106$ kHz during τ_2 (1.999 ms, 69 τ_c)), with the transmitter frequency centred at 11.0 ppm. 1024 transients were co-added for each of 64 t_1 FIDs, corresponding to a total experimental time of 92 h with a recycle of 5 s. The base contour is at 30 % of the maximum intensity.

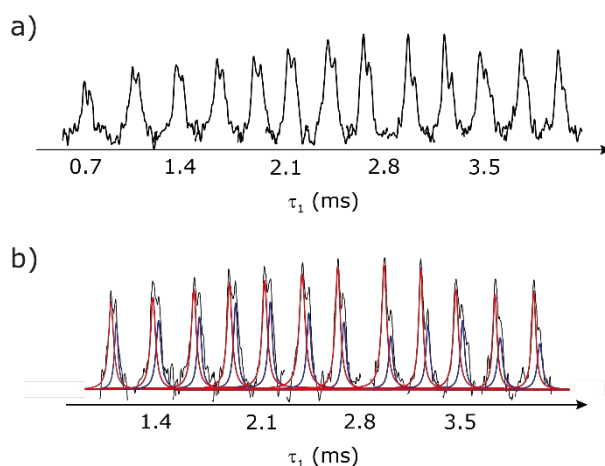


Figure 10. Dependence upon the first spin-echo duration, τ_1 , for a 1D-filtered ($t_1 = 0$) ^{15}N - 1H ($\nu_0 = 600$ MHz) CP (contact time = 3.7 ms)-Refocused INEPT MAS ($\nu_r = 60$ kHz) NMR spectrum for the dipeptide β -AspAla at natural isotopic abundance, recorded using $PMLG5_{mm}^{xx}$ 1H homonuclear decoupling ($\tau_{LG_expt} = 3.19 \mu s$, $\tau_{tilt} = 0.50 \mu s$, with $\nu_1 = 106$ kHz) for and $\tau_2 = 2.101$ ms (126 τ_r). All the spectra were acquired with 1024 co-added transients and a 1H transmitter offset of -2 kHz. A deconvolution of the NH (red) and NH_3 (blue) peaks is shown in (b).

4. Conclusions and Outlook

This paper has identified 1H homonuclear decoupling conditions for the $PMLG5_{mm}^{xx}$ supercycle at 60 kHz MAS that give enhanced resolution in a 1D NMR spectrum as compared to MAS alone. At 1 GHz, we report what we believe to be the first example of effective homonuclear decoupling achieved by using a rf nutation frequency lower than the MAS frequency. The establishing of 2D ^{15}N - 1H heteronuclear correlation for natural abundance solids using a 1H detected CP- J coupling based Refocused INEPT MAS NMR experiment^{26,38,39} has been demonstrated at 60 kHz MAS. The application of 1H homonuclear decoupling,



specifically the $PMLG5_{mm}^{\overline{xx}}$ supercycle^{26,39,57,85} results in a factor of nine sensitivity enhancement as compared to MAS alone. Notably, in our implementation at 500 MHz, a comparatively low ^1H nutation frequency, for a 1.3 mm rotor, of 100 kHz was used, with this being associated with a high chemical shift scaling factor of 0.82 and a large deviation from the ideal Lee-Goldburg condition. Future work could further probe the suitability and optimisation of such windowed and windowless decoupling sequences for applications involving spin-echo evolution. In addition, nutation-frequency-selective pulses that reduce rf inhomogeneity could also be explored.¹⁰⁴ The CP-Refocused INEPT pulse sequence is complementary to dipolar coupling-based double CP or the use of symmetry-based decoupling to establish ^{15}N - ^1H heteronuclear correlation under fast MAS.^{26,29,30,105} Note that the use of symmetry-based recoupling is more prone to t_1 noise.¹⁰⁶⁻¹⁰⁸ In future work, the extension of our approach to 100+ kHz MAS could be considered, noting an increasing number of applications to pharmaceuticals and other small and moderately sized organic molecules.^{9,109-115}

Acknowledgements

JT thanks Bruker and EPSRC for a PhD studentship through the EPSRC Centre for Doctoral Training in Molecular Analytical Science, grant number EP/L015307/1. The UK High-Field Solid-State NMR Facility used in this research was funded by EPSRC and BBSRC (EP/T015063/1), as well as, for the 1 GHz instrument, EP/R029946/1. The renewal of the 600 MHz solid-state NMR console (Avance NEO) was funded by BBSRC (BB/T018119/1), EPSRC and University of Warwick. We thank Dr Andrew P. Howes and Patrick Ruddy for supporting the operation of the Millburn House Magnetic Resonance Laboratory. Data for this study are provided as a supporting data set from the University of Warwick Research Datasets portal at https://wrap.warwick.ac.uk/**.



References

View Article Online
DOI: 10.1039/D2CP01041K

1. P. C. Vioglio, M. R. Chierotti and R. Gobetto, *Adv. Drug Deliv. Rev.*, 2017, **117**, 86.
2. E. Pindelska, A. Sokal and W. Kolodziejewski, *Adv. Drug Deliv. Rev.*, 2017, **117**, 111.
3. X. Lu, Y. Tsutsumi, C. Huang, W. Xu, S. R. Byrn, A. C. Templeton, A. V. Buevich, J.-P. Amoureux and Y. Su, *Phys. Chem. Chem. Phys.*, 2020, **22**, 13160.
4. M. Li, W. Xu and Y. Su, *Trac-Trends Anal. Chem.*, 2021, **135**, 116152.
5. J. R. Lewandowski, J.-N. Dumez, Ü. Akbey, S. Lange, L. Emsley and H. Oschkinat, *J. Phys. Chem. Lett.*, 2011, **2**, 2205.
6. D. Lacabanne, J. Boudet, A. A. Malär, P. Wu, R. Cadalbert, L. Salmon, F. H.-T. Allain, B. H. Meier and T. Wiegand, *J. Phys. Chem. B*, 2020, **124**, 11089.
7. V. Jirasko, A. Lends, N. A. Lakomek, M. L. Fogeron, M. E. Weber, A. A. Malär, S. Penzel, R. Bartenschlager, B. H. Meier and A. Böckmann, *Angew. Chem.*, 2021, **133**, 5399.
8. S. Bahri, R. Silvers, B. Michael, K. Jaudzems, D. Lalli, G. Casano, O. Ouari, A. Lesage, G. Pintacuda and S. Linse, *Proc. Natl. Acad. Sci.*, 2022, **119**, e2114413119.
9. U. Sternberg, R. Witter, I. Kuprov, J. M. Lamley, A. Oss, J. R. Lewandowski and A. Samoson, *J. Magn. Reson.*, 2018, **291**, 32.
10. Y. Nishiyama, *Solid State Nucl. Magn. Reson.*, 2016, **78**, 24.
11. A. A. Malär, S. Smith-Penzel, G.-M. Camenisch, T. Wiegand, A. Samoson, A. Böckmann, M. Ernst and B. H. Meier, *Phys. Chem. Chem. Phys.*, 2019, **21**, 18850.
12. M. Schledorn, A. A. Malär, A. Torosyan, S. Penzel, D. Klose, A. Oss, M. L. Org, S. Wang, L. Lecoq and R. Cadalbert, *Chembiochem*, 2020, **21**, 2540.
13. Z. Zhang, A. Oss, M.-L. Org, A. Samoson, M. Li, H. Tan, Y. Su and J. Yang, *J. Phys. Chem. Lett.*, 2020, **11**, 8077.
14. E. C.-Y. Yuan, S.-J. Huang, H.-C. Huang, J. Sinkkonen, A. Oss, M.-L. Org, A. Samoson, H.-C. Tai and J. C. C. Chan, *Chem. Commun.*, 2021, **57**, 4110.
15. Z. Gan, J. P. Amoureux and J. Trébosc, *Chem. Phys. Lett.*, 2007, **435**, 163.
16. S. Cavadini, S. Antonijevic, A. Lupulescu and G. Bodenhausen, *J. Magn. Reson.*, 2006, **182**, 168.
17. J. A. Jarvis, M. Concistre, I. M. Haies, R. W. Bounds, I. Kuprov, M. Carravetta and P. T. Williamson, *Phys. Chem. Chem. Phys.*, 2019, **21**, 5941.
18. M. Grüne, R. Luxenhofer, D. Iuga, S. P. Brown and A.-C. Pöppler, *J. Mater. Chem. B*, 2020, **8**, 6827.
19. K. Bártová, I. Císařová, A. Lyčka and M. Dračinský, *Dyes Pigment.*, 2020, **178**, 108342.
20. M. K. Pandey and Y. Nishiyama, *Phys. Chem. Chem. Phys.*, 2018, **20**, 25849.
21. A. Pugliese, M. Toresco, D. McNamara, D. Iuga, A. Abraham, M. Tobyn, L. E. Hawarden and F. Blanc, *Mol. Pharm.*, 2021, **18**, 3519.
22. A. S. Tatton, J. P. Bradley, D. Iuga and S. P. Brown, *Z. Phys. Chem.*, 2012, **226**, 1187.
23. Y. Ishii and R. Tycko, *J. Magn. Reson.*, 2000, 199.
24. Y. Ishii, J. P. Yesinowski and R. Tycko, *J. Am. Chem. Soc.*, 2001, **123**, 2921.
25. D. H. Zhou, G. Shah, C. Mullen, D. Sandoz and C. M. Rienstra, *Angew. Chem., Int. Ed. Engl.*, 2009, **48**, 1253.
26. S. M. Althaus, K. Mao, J. A. Stringer, T. Kobayashi and M. Pruski, *Solid State Nucl. Magn. Reson.*, 2014, **57-58**, 17.
27. A. Lesage, P. Charmont, S. Steuernagel and L. Emsley, *J. Am. Chem. Soc.*, 2000, **122**, 9739.
28. T. Kobayashi, K. Mao, P. Paluch, A. Nowak - Król, J. Sniechowska, Y. Nishiyama, D. T. Gryko, M. J. Potrzebowski and M. Pruski, *Angew. Chem.*, 2013, **125**, 14358.
29. S. L. Veinberg, K. E. Johnston, M. J. Jaroszewicz, B. M. Kispal, C. R. Mireault, T. Kobayashi, M. Pruski and R. W. Schurko, *Phys. Chem. Chem. Phys.*, 2016, **18**, 17713.
30. C. Guzmán-Afonso, Y.-I. Hong, H. Colaux, H. Iijima, A. Saitow, T. Fukumura, Y. Aoyama, S. Motoki, T. Oikawa and T. Yamazaki, *Nat. Commun.*, 2019, **10**, 3537.
31. E. K. Paulson, C. R. Morcombe, V. Gaponenko, B. Dancheck, R. A. Byrd and K. W. Zilm, *J. Am. Chem. Soc.*, 2003, **125**, 15831.
32. V. Chevelkov, K. Rehbein, A. Diehl and B. Reif, *Angew. Chem., Int. Ed. Engl.*, 2006, **45**, 3878.



33. D. H. Zhou, G. Shah, M. Cormos, C. Mullen, D. Sandoz and C. M. Rienstra, *J. Am. Chem. Soc.*, 2007, **129**, 11791. View Article Online
DOI: 10.1039/B2CP01041K
34. C. Fyfe, K. Wong-Moon, Y. Huang and H. Grondey, *J. Am. Chem. Soc.*, 1995, **117**, 10397.
35. O. Soubias, V. Réat, O. Saurel and A. Milon, *J. Magn. Reson.*, 2002, **158**, 143.
36. B. Alonso and D. Massiot, *J. Magn. Reson.*, 2003, **163**, 347.
37. B. Elena, A. Lesage, S. Steuernagel, A. Bockmann and L. Emsley, *J. Am. Chem. Soc.*, 2005, **127**, 17296.
38. K. Mao, J. W. Wiench, V. S.-Y. Lin and M. Pruski, *J. Magn. Reson.*, 2009, **196**, 92.
39. K. Mao and M. Pruski, *J. Magn. Reson.*, 2009, **201**, 165.
40. G. P. Holland, B. R. Cherry, J. E. Jenkins and J. L. Yarger, *J. Magn. Reson.*, 2010, **202**, 64.
41. P. K. Madhu, *Solid State Nucl. Magn. Reson.*, 2009, **35**, 2.
42. K. R. Mote, V. Agarwal and P. K. Madhu, *Prog. Nucl. Magn. Reson. Spectrosc.*, 2016, **97**, 1.
43. P. Hodgkinson, *Annu. Rep. NMR Spectrosc.*, 2011, **72**, 185.
44. E. Vinogradov, P. K. Madhu and S. Vega, *New Techniques in Solid-State NMR*, 2005, 33.
45. M. Lee and W. I. Goldberg, *Phys. Rev.*, 1965, **140**, A1261.
46. M. H. Levitt, A. C. Kolbert, A. Bielecki and D. J. Ruben, *Solid State Nucl. Magn. Reson.*, 1993, **2**, 151.
47. M. Hohwy and N. C. Nielsen, *J. Chem. Phys.*, 1997, **106**, 7571.
48. M. Hohwy, P. Bower, H. Jakobsen and N. Nielsen, *Chem. Phys. Lett.*, 1997, **273**, 297.
49. E. Vinogradov, P. K. Madhu and S. Vega, *Chem. Phys. Lett.*, 1999, **314**, 443.
50. D. Sakellariou, A. Lesage, P. Hodgkinson and L. Emsley, *Chem. Phys. Lett.*, 2000, 253.
51. P. Madhu, X. Zhao and M. H. Levitt, *Chem. Phys. Lett.*, 2001, **346**, 142.
52. M. E. Halse and L. Emsley, *Phys. Chem. Chem. Phys.*, 2012, **14**, 9121.
53. F. M. Paruzzo and L. Emsley, *J. Magn. Reson.*, 2019, **309**, 106598.
54. C. Coelho, J. Rocha, P. Madhu and L. Mafra, *J. Magn. Reson.*, 2008, **194**, 264.
55. I. Schnell, S. P. Brown, H. Y. Low, H. Ishida and H. W. Spiess, *J. Am. Chem. Soc.*, 1998, **120**, 11784.
56. J.-P. Amoureux, B. Hu, J. Trébosc, Q. Wang, O. Lafon and F. Deng, *Solid State Nucl. Magn. Reson.*, 2009, **35**, 19.
57. Y. Nishiyama, X. Lu, J. Trebosc, O. Lafon, Z. Gan, P. K. Madhu and J. P. Amoureux, *J. Magn. Reson.*, 2012, **214**, 151.
58. E. Salager, J.-N. Dumez, R. S. Stein, S. Steuernagel, A. Lesage, B. Elena-Herrmann and L. Emsley, *Chem. Phys. Lett.*, 2010, **498**, 214.
59. M. Leskes, S. Steuernagel, D. Schneider, P. K. Madhu and S. Vega, *Chem. Phys. Lett.*, 2008, **466**, 95.
60. J.-P. Amoureux, B. Hu and J. Trébosc, *J. Magn. Reson.*, 2008, **193**, 305.
61. Z. Gan, P. Madhu, J.-P. Amoureux, J. Trébosc and O. Lafon, *Chem. Phys. Lett.*, 2011, **503**, 167.
62. E. Salager, R. S. Stein, S. Steuernagel, A. Lesage, B. Elena and L. Emsley, *Chem. Phys. Lett.*, 2009, **469**, 336.
63. B. Gerstein, R. Pembleton, R. Wilson and L. Ryan, *J. Chem. Phys.*, 1977, **66**, 361.
64. E. Salager, J. N. Dumez, L. Emsley and M. H. Levitt, *J. Magn. Reson.*, 2011, **212**, 11.
65. M. Leskes, P. K. Madhu and S. Vega, *J. Magn. Reson.*, 2009, **199**, 208.
66. R. Ramesh and M. S. Krishnan, *J. Chem. Phys.*, 2001, **114**, 5967.
67. S. Hayashi and K. Hayamizu, *Bull. Chem. Soc. Jpn.*, 1991, **64**, 685.
68. E. K. Corlett, H. Blade, L. P. Hughes, P. J. Sidebottom, D. Walker, R. I. Walton and S. P. Brown, *Crystengcomm*, 2019, **21**, 3502.
69. S. Hayashi and K. Hayamizu, *Bull. Chem. Soc. Jpn.*, 1991, **64**, 688.
70. R. K. Harris, E. D. Becker, S. M. C. De Menezes, P. Granger, R. E. Hoffman and K. W. Zilm, *Pure Appl. Chem.*, 2008, **80**, 59.
71. G. E. Martin and C. E. Hadden, *J. Nat. Prod.*, 2000, **63**, 543.
72. B. Meier, *Chem. Phys. Lett.*, 1992, **188**, 201.
73. S. Laage, J. R. Sachleben, S. Steuernagel, R. Pierattelli, G. Pintacuda and L. Emsley, *J. Magn. Reson.*, 2009, **196**, 133.
74. G. Metz, X. Wu and S. O. Smith, *J. Magn. Reson.*, 1994, **110**, 219.
75. D. H. Zhou and C. M. Rienstra, *J. Magn. Reson.*, 2008, **192**, 167.



76. M. Ernst, M. A. Meier, T. Tuherm, A. Samoson and B. H. Meier, *J. Am. Chem. Soc.*, 2004, **126**, 4764. View Article Online
DOI: 10.1039/B2CP01041K
77. A. Shaka, J. Keeler and R. Freeman, *J. Magn. Reson. (1969)*, 1983, **53**, 313.
78. Z. Zhou, R. Kummerle, X. Qiu, D. Redwine, R. Cong, A. Taha, D. Baugh and B. Winniford, *J. Magn. Reson.*, 2007, **187**, 225.
79. A. Lesage, S. Steuernagel and L. Emsley, *J. Am. Chem. Soc.*, 1998, **120**, 7095.
80. A. S. Tatton, I. Frantsuzov, S. P. Brown and P. Hodgkinson, *J. Chem. Phys.*, 2012, **136**, 084503.
81. A. Lesage, L. Emsley, M. Chabanas, C. Coperet and J.-M. Basset, *Angew. Chem.*, 2002, **114**, 4717.
82. M. P. Hanrahan, E. L. Fought, T. L. Windus, L. M. Wheeler, N. C. Anderson, N. R. Neale and A. J. Rossini, *Chem. Mat.*, 2017, **29**, 10339.
83. R. W. Dorn, E. A. Marro, M. P. Hanrahan, R. S. Klausen and A. J. Rossini, *Chem. Mat.*, 2019, **31**, 9168.
84. B. J. Ryan, M. P. Hanrahan, Y. Wang, U. Ramesh, C. K. A. Nyamekye, R. D. Nelson, Z. Liu, C. Huang, B. Whitehead, J. Wang, L. T. Roling, E. A. Smith, A. J. Rossini and M. G. Panthani, *Chem. Mat.*, 2020, **32**, 795.
85. M. Leskes, P. K. Madhu and S. Vega, *Chem. Phys. Lett.*, 2007, **447**, 370.
86. M. Mehring and J. Waugh, *Phys. Rev. B*, 1972, **5**, 3459.
87. A. Bielecki, A. C. Kolbert and M. H. Levitt, *Chem. Phys. Lett.*, 1989, **155**, 341.
88. E. Vinogradov, P. K. Madhu and S. Vega, *Chem. Phys. Lett.*, 2002, **354**, 193.
89. M. Leskes, P. K. Madhu and S. Vega, *J. Chem. Phys.*, 2006, **125**, 124506.
90. S. Paul, R. S. Thakur, M. Goswami, A. C. Sauerwein, S. Mamone, M. Concistre, H. Forster, M. H. Levitt and P. K. Madhu, *J. Magn. Reson.*, 2009, **197**, 14.
91. V. E. Zorin, M. Ernst, S. P. Brown and P. Hodgkinson, *J. Magn. Reson.*, 2008, **192**, 183.
92. C. Coelho, J. Rocha, P. K. Madhu and L. Mafra, *J. Magn. Reson.*, 2008, **194**, 264.
93. K. Mao and M. Pruski, *J. Magn. Reson.*, 2010, **203**, 144.
94. S. Hafner and H. W. Spiess, *J. Magn. Reson. Ser. A*, 1996, **121**, 160.
95. E. Vinogradov, P. Madhu and S. Vega, *Chem. Phys. Lett.*, 2000, **329**, 207.
96. A. Lesage, D. Sakellariou, S. Hediger, B. Eléna, P. Charmont, S. Steuernagel and L. Emsley, *J. Magn. Reson.*, 2003, **163**, 105.
97. J. S. Waugh, L. M. Huber and U. Haeberlen, *Phys. Rev. Lett.*, 1968, **20**, 180.
98. A. J. Vega, *J. Magn. Reson.*, 2004, **170**, 22.
99. A. Lesage, M. Bardet and L. Emsley, *J. Am. Chem. Soc.*, 1999, **121**, 10987.
100. V. E. Zorin, S. P. Brown and P. Hodgkinson, *J. Chem. Phys.*, 2006, **125**, 144508.
101. L. Bosman, P. K. Madhu, S. Vega and E. Vinogradov, *J. Magn. Reson.*, 2004, **169**, 39.
102. A. S. Tatton, T. N. Pham, F. G. Vogt, D. Iuga, A. J. Edwards and S. P. Brown, *Crystengcomm*, 2012, **14**, 2654.
103. K. Maruyoshi, D. Iuga, A. E. Watts, C. E. Hughes, K. D. Harris and S. P. Brown, *J. Pharm. Sci.*, 2017, **106**, 3372.
104. K. Aebischer, N. Wili, Z. Tošner and M. Ernst, *Magn. Reson.*, 2020, **1**, 187.
105. F. A. Perras, T. W. Goh, L.-L. Wang, W. Huang and M. Pruski, *Solid State Nucl. Magn. Reson.*, 2019, **98**, 12.
106. A. J. Robertson, M. K. Pandey, A. Marsh, Y. Nishiyama and S. P. Brown, *J. Magn. Reson.*, 2015, **260**, 89.
107. M. Shen, S. Wegner, J. Trébosc, B. Hu, O. Lafon and J.-P. Amoureux, *Solid State Nucl. Magn. Reson.*, 2017, **87**, 111.
108. A. Venkatesh, X. Luan, F. A. Perras, I. Hung, W. Huang and A. J. Rossini, *Phys. Chem. Chem. Phys.*, 2020, **22**, 20815.
109. Y. Nishiyama, M. Malon, Y. Ishii and A. Ramamoorthy, *J. Magn. Reson.*, 2014, **244**, 1.
110. Y. Nishiyama, T. Kobayashi, M. Malon, D. Singappuli-Arachchige, I. Slowing and M. Pruski, *Solid State Nucl. Magn. Reson.*, 2015, **66**, 56.
111. J. Struppe, C. M. Quinn, M. Lu, M. Wang, G. Hou, X. Lu, J. Kraus, L. B. Andreas, J. Stanek and D. Lalli, *Solid State Nucl. Magn. Reson.*, 2017, **87**, 117.
112. J. Struppe, C. M. Quinn, S. Sarkar, A. M. Gronenborn and T. Polenova, *Mol. Pharm.*, 2019, **17**, 674.



113. R. Zhang, Y.-I. Hong, T. Ravula, Y. Nishiyama and A. Ramamoorthy, *J. Magn. Reson.*, 2020, **313**, 106717. View Article Online
DOI: 10.1039/D2CP01041K
114. P. Moutzouri, F. M. Paruzzo, B. Simoes de Almeida, G. Stevanato and L. Emsley, *Angew. Chem., Int. Ed. Engl.*, 2020, **59**, 6235.
115. P. Moutzouri, B. Simões de Almeida, D. Torodii and L. Emsley, *J. Am. Chem. Soc.*, 2021, **143**, 9834.

